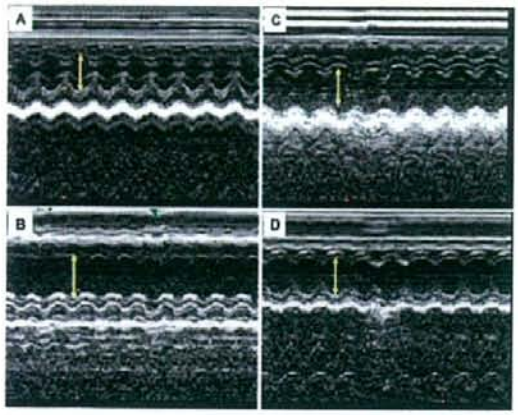

Figure 7. Effect of endothelial CysLT$_2$R overexpression on left ventricular wall and chamber dimensions. **A–D:** Representative M-mode frames from the mid-papillary region of tg (**A, B**) and ntg (**C, D**) before (**A, C**) and 2 weeks after (**B, D**) acute I/R injury. **Arrow** indicates width of the LV chamber.

inflammatory and adhesion molecules, leading to increased vascular permeability, inflammatory cell infiltration, and platelet adhesion and thrombus formation.[5] CysLTs are major inflammatory mediators and activation of endothelial CysLT$_2$R markedly increases vascular permeability in transgenic mice.[16] We now report that myocardial injury in response to acute I/R is exacerbated in endothelium-targeted CysLT$_2$R transgenic mice, in association with increased coronary vascular permeability, inflammatory cell infiltration, and heightened myocyte loss through apoptosis.

CysLT synthesis increases in humans[20] with myocardial infarction. Furthermore, pretreatment with leukotriene biosynthesis inhibitors, AA-861 or Bay X1005, reduces neutrophil influx and infarct size after I/R injury in rats[39] and rabbits,[40] respectively, and intravenous infusion of a CysLT receptor antagonist LY-171883 at reperfusion decreases infarct size and improves LV functional recovery after myocardial infarction in cats.[41] In addition, recent linkage analysis studies revealed increased risk of stroke and myocardial infarction in some ethnic groups harboring a distinct haplotype in the *ALOX5AP* gene encoding 5-lipoxygenase-activating protein.[42] Thus, it is plausible in the current study that CysLTs released from resident and/or circulating inflammatory cells or synthesized by transcellular pathways between interacting neutrophils and endothelial cells[40,43] may activate CysLT$_2$Rs in vascular endothelium to promote endothelial leakage and subsequent myocardial damage. CysLTs influence the adhesion of neutrophils to endothelium by up-regulating adhesion molecules[44,45] and may also act as chemotactic factors in recruitment of leukocytes to the infarcted myocardium. There is compelling evidence that activation of CysLT$_2$R in cultured human endothelial cells leads to activation of a distinct set of immediate-early gene signatures[46] including the transcription factor Egr-1 and a variety of signaling and adhesion molecules that have been shown to participate in ischemic stress and reperfusion injury in mice.[47] In agreement with these findings, the expression of Egr-1, as well as ICAM and VCAM-1 genes, were elevated in the present study after activation of the human transgene in vascular endothelium, suggesting that they may contribute to the enhanced endothelial permeability and neutrophil infiltration in the infarcted myocardium of tg mice.

To examine the relative impact of transgenic endothelial overexpression of CysLT$_2$ receptor vis-à-vis native CysLT$_2$ expression after I/R, a number of tests were performed including analysis of the expression level of CysLT$_1$ and CysLT$_2$ receptors before and after injury (Figure 1), as well as comparative analysis of treatment with the dual CysLT$_1$/CysLT$_2$ receptor antagonist Bay-u9773, combined with infarction analysis of 5LO/leukotriene-deficient mice (Figure 2). Real-time PCR analysis indicated low levels of native murine CysLT$_1$ and CysLT$_2$ receptors in sham-operated mouse hearts and early after I/R (3 hours) with significantly higher levels of both receptors 48 hours after I/R. We speculate that the increased CysLT$_1$R levels at 48 hours of I/R are attributable to infiltrating mononuclear leukocytes, a predominant cell type at this time point[32] and cells known to express this receptor subtype.[48] Based on the blue X-gal/LacZ staining in heart tissue as a surrogate for CysLT$_2$R expression, enhanced expression of this receptor subtype after 48 hours of I/R in the infarct and peri-infarct zones was observed (Figure 1). Although the specific cell types expressing the induced receptor were not positively identified, several cell types including vascular smooth muscle[12] and endothelial cells,[15] Purkinje conducting cells,[11]

Table 1. Two-Dimensional Echocardiographic Analysis of Left Ventricular Wall and Chamber Dimension before and 2 Weeks after Acute Myocardial I/R in CysLT$_2$R Transgenic and Nontransgenic Mice

	Pre-ischemia/reperfusion		Post-ischemia/reperfusion		% change from pre I/R	
	ntg	tg	ntg	tg	ntg	tg
LVDd (mm)	0.350 ± 0.010	0.389 ± 0.0120*	0.378 ± 0.0087	0.424 ± 0.0300	8.6 ± 4.4	8.8 ± 6.5
LVDs (mm)	0.200 ± 0.0090	0.229 ± 0.0173	0.220 ± 0.0185	0.27 ± 0.0342	11.5 ± 10.2	20.9 ± 15.9
IVSd (mm)	0.0751 ± 0.0030	0.0707 ± 0.0022	0.0727 ± 0.0025	0.0712 ± 0.0008	−2.6 ± 4.0	1.3 ± 3.8
IVSs (mm)	0.127 ± 0.0047	0.125 ± 0.0083	0.118 ± 0.0085	0.103 ± 0.0067†	−6.1 ± 8.8	−16.9 ± 4.3
PWd (mm)	0.0719 ± 0.0017	0.0763 ± 0.0044	0.0811 ± 0.0045	0.0867 ± 0.0041	13.9 ± 8.4	16.7 ± 11.2
PWs (mm)	0.124 ± 0.0052	0.125 ± 0.0044	0.143 ± 0.0148	0.148 ± 0.0060†	15.9 ± 11.4	19.6 ± 7.6
HR (bpm)	472 ± 17	479 ± 30	476 ± 21	481 ± 40	1.2 ± 4.9	0.30 ± 4.6

LVDd, left ventricular chamber diameter at diastole; LVDs, left ventricular chamber diameter at systole; IVSd, interventricular septum thickness at diastole; IVSs, interventricular septum thickness at systole; PWd, posterior wall thickness at diastole; PWs, posterior wall thickness at systole; HR, heart rate. *$P < 0.05$, tg versus ntg by unpaired *t*-test; †$P < 0.05$, pre-I/R versus post-I/R by paired *t*-test.

Table 2. Left Ventricular Function in Control $CysLT_2R$-Transgenic and Nontransgenic Mice and 2 Weeks after Acute Myocardial I/R Injury

	ntg				tg			
	Control ($n = 6$)		I/R ($n = 5$)		Control ($n = 5$)		I/R ($n = 5$)	
	Before DB	After DB	Before DB	After DB	Before DB	After DB	Before DB	After DB
Heart rate, beats/minute	633 ± 14	709 ± 17*	616 ± 26	664 ± 44	575 ± 13†	642 ± 11*‡	519 ± 32‡	522 ± 39†‡
LV function								
LV peak pressure, mmHg	71 ± 2	138 ± 13*	69 ± 4	72 ± 3	74 ± 4	130 ± 14*	70 ± 4	83 ± 8
LVESP, mmHg	70 ± 2	138 ± 13*	68 ± 4	71 ± 3	72 ± 4	130 ± 14*	70 ± 4*	83 ± 8†
LVEDP, mmHg	3. ± 0	5 ± 1	3 ± 0.3	4 ± 0.4	5 ± 1	7 ± 1*	4 ± 0.6	4 ± 0.2
LV +dP/dt, mmHg/second	5636 ± 320	16,046 ± 1281*	6409 ± 425	9952 ± 1557*†	6571 ± 604	13,921 ± 1867*	4896 ± 569	7412 ± 1728†
LV −dP/dt, min Hg/second	−6058 ± 423	−10,377 ± 648*	−6624 ± 489	−6454 ± 397†	−6267 ± 621	−9144 ± 680*	−4865 ± 662	−5370 ± 735†
τ, ms	6.37 ± 0.44	5.10 ± 0.19*	5.91 ± 0.33	4.94 ± 0.17*	5.76 ± 0.22	5.77 ± 0.20‡	7.91 ± 0.82†	7.17 ± 0.77‡

DB, dobutamine; LV, left ventricle; LVESP, left ventricular end-systolic pressure; LVEDP, left ventricular end-diastolic pressure; LV +dP/dt, maximal value of the first derivative of LV pressure; LV −dP/dt, minimal value of the first derivative of LV pressure; τ, time constant for isovolumic relaxation.
*$P < 0.05$ after DB versus before DB; †$P < 0.05$, control versus I/R; ‡$P < 0.05$ tg versus ntg.

mesenchymal stem cells, and perhaps some leukocytes are possible candidates.

Bay-u9773 is a nonspecific antagonist of $CysLT_1R$ and $CysLT_2R$, rendering it difficult to determine the precise contributions of each receptor subtype to ischemic injury. This is further complicated by the recent discovery of a third CysLT receptor subtype termed GPR17, that can bind $CysLT_1R$ antagonists and was found to participate in focal rat brain ischemic injury.[10] Therefore, depending on the organ and tissue-specific vascular beds, various CysLT receptor subtypes might contribute to inflammatory vascular permeability changes in ischemic injury. In our studies, absence of leukotriene ligand to $CysLT_2R$, as represented in 5LO-deficient mice, and in preliminary studies with the recently acquired $CysLT_2R$-deficient LacZ mice ($n = 3$, data not shown), lack of ligand/receptor did not significantly influence myocardial injury compared to ntg mice. These data are consistent with those in a recent study showing that I/R injury did not differentially affect infarct size in 5LO-deficient mice compared to wild-type controls[49] but apparently not in agreement with the studies mentioned above with leukotriene biosynthesis inhibitors.[39,40] Moreover, the finding that Bay-u9773 did not reduce infarct size below baseline levels in ntg mice suggests that endogenous $CysLT_2R$ does not play a significant role in I/R injury in contrast to the transgenic overexpression of the receptor. However, the observation that I/R induces murine $CysLT_2R$ in our study at 48 hours, along with a recent report examining $CysLT_2R$ expression in human brain tissue finding increased expression in microvascular endothelium after traumatic injury,[50] warrants further study to examine the pathophysiological sequelae of induction of $CysLT_2R$.

The mechanism by which endothelial $CysLT_2R$ overexpression leads to increased myocyte apoptosis is not known. To our knowledge no direct role of $CysLT_2R$ in cardiomyocyte apoptosis has been established. The cascade of events leading to myocyte apoptosis during I/R involves the activation of both the intrinsic mitochondrial proapoptotic pathway as well as the extrinsic pathway mediated by cytokine activation of death receptors.[51] Myocytes are particularly prone to apoptosis during reperfusion,[52] where up to 30% in the risk area may undergo apoptosis in the first few hours after reperfusion. The events of reperfusion that lead to cardiomyocyte apoptosis have not been fully elucidated. However, reactive oxygen species and cytokines produced by infiltrating inflammatory cells appear to play a central role in activating apoptotic pathways in myocytes.[52,53] For example, genetic mouse models harboring deletions of tumor necrosis factor-α and CD18 genes show reduced infarct size in response to I/R in association with decreased neutrophil infiltration, whereas null mice for the anti-oxidant gene heme oxygenase-1 have increased infarct size and reduced LV recovery in parallel with a decrease in antioxidant load.[52] In the current study, the enhanced influx of $CD45^+$ leukocytes, presumably mostly neutrophils, after reperfusion in $CysLT_2R$ tg mice could potentially contribute to the enhanced myocyte apoptosis seen in these animals by a similar mechanism; however, additional mechanisms may also be at play. Regardless of mechanism, the increased apoptosis in tg mice would predictably lead to greater long-term loss of myocardial contractile mass, resulting in LV chamber remodeling and impairment of contractile function. Indeed, in the current study, $CysLT_2R$ mice show accelerated LV remodeling, highlighted by decreased anterior wall thickness and increased LV systolic dimensions 2 weeks after reperfusion. Typically, LV remodeling in mice with reperfused myocardium is slow and often absent,[37]

unless a significant amount of the LV (>40% of the area at risk) is infarcted. Our results indicate that tg CysLT$_2$R mice had significantly larger infarcts than the ntg counterparts. We presume that the heightened apoptosis is, at least partially, responsible for the larger infarct sizes and subsequent LV remodeling in these mice.

As expected, LV remodeling in tg mice was accompanied by impaired LV function after reperfusion. We believe that this is directly attributable to the greater myocyte loss in tg mice, because basal LV function and responsiveness to β-adrenergic stimulation did not differ significantly between the two groups of animals. In contrast, ntg mice were able to preserve LV function after reperfusion because of the significantly smaller infarcts and absence of negative remodeling. Interestingly, both genotypes showed marked refractoriness to dobutamine after reperfusion. The mechanism underlying this lack of response appears to be unrelated to CysLT$_2$R overexpression, because it is also present in ntg controls. β-Adrenergic receptor desensitization usually occurs after myocardial infarction as the sympathetic nervous system attempts to maintain hemodynamic homeostasis. However, desensitization usually occurs throughout a longer time course than in the current studies, and is unlikely to be the explanation for the postreperfusion refractoriness to dobutamine.

In summary, the results of the current study indicate that endothelial-targeted overexpression of CysLT$_2$R exacerbates myocardial injury after ischemia reperfusion in association with increased inflammatory cell infiltration and cardiomyocyte apoptosis. Inhibition of endothelial CysLT$_2$R activity should be explored further as a potential strategy for myocardial protection.

Acknowledgments

We thank Karoline Machado and the staff at the Queen's University Transgenic Animal Facility for performing the embryo transfer procedures to obtain CysLT$_2$R-deficient LacZ mice. Yiqun Hui is kindly acknowledged for supplying the CysLT$_2$R transgenic mice.

References

1. Buja LM: Myocardial ischemia and reperfusion injury. Cardiovasc Pathol 2005, 14:170–175
2. Moens AL, Claeys MJ, Timmermans JP, Vrints CJ: Myocardial ischemia/reperfusion-injury, a clinical view on a complex pathophysiological process. Int J Cardiol 2005, 100:179–190
3. Park JL, Lucchesi BR: Mechanisms of myocardial reperfusion injury. Ann Thorac Surg 1999, 68:1905–1912
4. Di Napoli P, Taccardi AA, De Caterina R, Barsotti A: Pathophysiology of ischemia-reperfusion injury: experimental data. Ital Heart J 2002, 3(Suppl 4):24S–28S
5. Lefer AM, Tsao PS, Lefer DJ, Ma XL: Role of endothelial dysfunction in the pathogenesis of reperfusion injury after myocardial ischemia. FASEB J 1991, 5:2029–2034
6. Funk CD: Prostaglandins and leukotrienes: advances in eicosanoid biology. Science 2001, 294:1871–1875
7. Funk CD: Leukotriene modifiers as potential therapeutics for cardiovascular disease. Nat Rev Drug Disc 2005, 4:664–672
8. Hui Y, Funk CD: Cysteinyl leukotriene receptors. Biochem Pharmacol 2002, 64:1549–1557
9. Folco G, Rossoni G, Buccellati C, Berti F, Maclouf J, Sala A: Leukotrienes in cardiovascular diseases. Am J Respir Crit Care Med 2000, 161:S112–S116
10. Ciana P, Fumagalli M, Trincavelli ML, Verderio C, Rosa P, Lecca D, Ferrario S, Parravicini C, Capra V, Gelosa P, Guerrini U, Belcredito S, Cimino M, Sironi L, Tremoli E, Rovati GE, Martini C, Abbracchio MP: The orphan receptor GPR17 identified as a new dual uracil nucleotides/cysteinyl-leukotrienes receptor. EMBO J 2006, 25:4615–4627
11. Heise CE, O'Dowd BF, Figueroa DJ, Sawyer N, Nguyen T, Im DS, Stocco R, Bellefeuille JN, Abramovitz M, Cheng R, Williams DL Jr, Zeng Z, Liu Q, Ma L, Clements MK, Coulombe N, Liu Y, Austin CP, George SR, O'Neill GP, Metters KM, Lynch KR, Evans JF: Characterization of the human cysteinyl leukotriene 2 receptor. J Biol Chem 2000, 275:30531–30536
12. Takasaki J, Kamohara M, Matsumoto M, Saito T, Sugimoto T, Ohishi T, Ishii H, Ota T, Nishikawa T, Kawai Y, Masuho Y, Isogai T, Suzuki Y, Sugano S, Furuichi K: The molecular characterization and tissue distribution of the human cysteinyl leukotriene CysLT(2) receptor. Biochem Biophys Res Commun 2000, 274:316–322
13. Lötzer K, Spanbroek R, Hildner M, Urbach A, Heller R, Bretschneider E, Galczenski H, Evans JF, Habenicht AJ: Differential leukotriene receptor expression and calcium responses in endothelial cells and macrophages indicate 5-lipoxygenase-dependent circuits of inflammation and atherogenesis. Arterioscler Thromb Vasc Biol 2003, 23:e32–e36
14. Kamohara M, Takasaki J, Matsumoto M, Matsumoto SI, Saito T, Soga T, Matsushime H, Furuichi K: Functional characterization of cysteinyl leukotriene CysLT(2) receptor on human coronary artery smooth muscle cells. Biochem Biophys Res Commun 2001, 287:1088–1092
15. Hui Y, Yang G, Galczenski H, Figueroa DJ, Austin CP, Copeland NG, Gilbert DJ, Jenkins NA, Funk CD: The murine cysteinyl leukotriene 2 (CysLT2) receptor, cDNA and genomic cloning, alternative splicing, and in vitro characterization. J Biol Chem 2001, 276:47489–47495
16. Hui Y, Cheng Y, Smalera I, Jian W, Goldhahn L, Fitzgerald GA, Funk CD: Directed vascular expression of human cysteinyl leukotriene 2 receptor modulates endothelial permeability and systemic blood pressure. Circulation 2004, 110:3360–3366
17. Kanaoka Y, Boyce JA: Cysteinyl leukotrienes and their receptors: cellular distribution and function in immune and inflammatory responses. J Immunol 2004, 173:1503–1510
18. Frangogiannis NG, Smith CW, Entman ML: The inflammatory response in myocardial infarction. Cardiovasc Res 2002, 53:31–47
19. Barst S, Mullane K: The release of a leukotriene D4-like substance following myocardial infarction in rabbits. Eur J Pharmacol 1985, 114:383–387
20. Carry M, Korley V, Willerson JT, Weigelt L, Ford-Hutchinson AW, Tagari P: Increased urinary leukotriene excretion in patients with cardiac ischemia. In vivo evidence for 5-lipoxygenase activation. Circulation 1992, 85:230–236
21. Yu GL, Wei EQ, Zhang SH, Xu HM, Chu LS, Zhang WP, Zhang Q, Chen Z, Mei RH, Zhao MH: Montelukast, a cysteinyl leukotriene receptor-1 antagonist, dose- and time-dependently protects against focal cerebral ischemia in mice. Pharmacology 2005, 73:31–40
22. Fang SH, Zhou Y, Chu LS, Zhang WP, Wang ML, Yu GL, Peng F, Wei EQ: Spatio-temporal expression of cysteinyl leukotriene receptor-2 mRNA in rat brain after focal cerebral ischemia. Neurosci Lett 2007, 412:78–83
23. Sener G, Sehirli O, Velioglu-Ogunc A, Cetinel S, Gedik N, Caner M, Sakarcan A, Yegen BC: Montelukast protects against renal ischemia/reperfusion injury in rats. Pharmacol Res 2006, 54:65–71
24. Chen XS, Sheller JR, Johnson EN, Funk CD: Role of leukotrienes revealed by targeted disruption of the 5-lipoxygenase gene. Nature 1994, 372:179–182
25. Tarnavski O, McMullen JR, Schinke M, Nie Q, Kong S, Izumo S: Mouse cardiac surgery: comprehensive techniques for the generation of mouse models of human diseases and their application for genomic studies. Physiol Genom 2004, 16:349–360
26. Liu X, Wei J, Peng DH, Layne MD, Yet SF: Absence of heme oxygenase-1 exacerbates myocardial ischemia/reperfusion injury in diabetic mice. Diabetes 2005, 54:778–784
27. Petzelbauer P, Zacharowski PA, Miyazaki Y, Friedl P, Wickenhauser G, Castellino FJ, Groger M, Wolff K, Zacharowski K: The fibrin-derived peptide Bbeta15-42 protects the myocardium against ischemia-reperfusion injury. Nat Med 2005, 11:298–304
28. Schumacher J, Binkowski K, Dendorfer A, Klotz KF: Organ-specific

extravasation of albumin-bound Evans blue during nonresuscitated hemorrhagic shock in rats. Shock 2003, 20:565–568
29. Younger JG, Sasaki N, Delgado J, Ko AC, Nghiem TX, Waite MD, Till GO, Ward PA: Systemic and lung physiological changes in rats after intravascular activation of complement. J Appl Physiol 2001, 90:2289–2295
30. Harja E, Bucciarelli LG, Lu Y, Stern DM, Zou YS, Schmidt AM, Yan SF: Early growth response-1 promotes atherogenesis: mice deficient in early growth response-1 and apolipoprotein E display decreased atherosclerosis and vascular inflammation. Circ Res 2004, 94:333–339
31. Takahashi T, Tang T, Lai NC, Roth DM, Rebolledo B, Saito M, Lew WY, Clopton P, Hammond HK: Increased cardiac adenylyl cyclase expression is associated with increased survival after myocardial infarction. Circulation 2006, 114:388–396
32. Dewald O, Ren G, Duerr GD, Zoerlein M, Klemm C, Gersch C, Tincey S, Michael LH, Entman ML, Frangogiannis NG: Of mice and dogs: species-specific differences in the inflammatory response following myocardial infarction. Am J Pathol 2004, 164:665–677
33. Okada Y, Scott G, Ray MK, Mishina Y, Zhang Y: Histone demethylase JHDM2A is critical for Tnp1 and Prm1 transcription and spermatogenesis. Nature 2007, 450:119–123
34. Liu X, Simpson JA, Brunt KR, Ward CA, Hall SR, Kinobe RT, Barrette V, Tse MY, Pang SC, Pachori AS, Dzau VJ, Ogunyankin K, Melo LG: Pre-emptive heme oxygenase-1 gene delivery reveals reduced mortality and preservation of left ventricular function one year after acute myocardial infarction. Am J Physiol 2007, 293:H48–H59
35. Hall SR, Wang L, Milne B, Hong M: Left ventricular dysfunction after acute intracranial hypertension is associated with increased hydroxyl free radical production, cardiac ryanodine hyperphosphorylation, and troponin I degradation. J Heart Lung Transplant 2005, 24:1639–1649
36. Anversa P, Beghi C, Kikkawa Y, Olivetti G: Myocardial infarction in rats. Infarct size, myocyte hypertrophy and capillary growth. Circ Res 1986, 58:26–37
37. De Celle T, Cleutjens JP, Balnkesteijn WM, Debets JJ, Smits JF, Janssen BJ: Long-term structural and functional consequences of cardiac ischemia-reperfusion injury in vivo in mice. Exp Physiol 2004, 89:605–615
38. Rubanyi GM: The role of endothelium in cardiovascular homeostasis and disease. J Cardiovasc Pharmacol 1993, 22:S1–S4
39. Sasaki K, Ueno A, Kswamura M, Katori M, Shigehiro S, Kikawada R: Reduction of myocardial infarct size in rats by selective 5-lipooxygenase inhibitor (AA-861). Adv Prostglandin Thromboxane Leukot Res 1987, 17A:381–383
40. Rossoni G, Sala A, Berti F, Testa T, Buccellati C, Molta C, Muller-Peddinghaus R, Maclouf J, Folco GC: Myocardial protection by the leukotriene synthesis inhibitor BAY X1005: importance of transcellular biosynthesis of cysteinyl-leukotrienes. J Pharmacol Exp Ther 1996, 276:335–341
41. Hock CE, Beck LD, Papa LA: Peptide leukotriene antagonism in myocardial ischemia and reperfusion. Cardiovasc Res 1992, 26:1206–1211
42. Helgadottir A, Manolescu A, Thorleifsson G, Gretarsdottir S, Jonsdottir H, Thorsteinsdottir U, Samani NJ, Gudmundsson G, Grant SF, Thorgeirsson G, Sveinbjornsdottir S, Valdimarsson EM, Matthiasson SE, Johannsson H, Gudmundsdottir O, Gurney ME, Sainz J, Thorhallsdottir M, Andresdottir M, Frigge ML, Topol EJ, Kong A, Gudnason V, Hakonarson H, Gulcher JR, Stefansson K: The gene encoding 5-lipoxygenase activating protein confers risk of myocardial infarction and stroke. Nat Genet 2004, 36:233–239
43. Sala A, Folco G: Neutrophils, endothelial cells, and cysteinyl leukotrienes: a new approach to neutrophil-dependent inflammation? Biochem Biophys Res Commun 2001, 283:1003–1006
44. Pedersen KE, Bochner BS, Undem BJ: Cysteinyl leukotrienes induce P-selectin expression in human endothelial cells via a non-CysLT1 receptor-mediated mechanism. J Pharmacol Exp Ther 1997, 281:655–662
45. Di Gennaro A, Carnini C, Buccellati C, Ballerio R, Zarini S, Fumagalli F, Viappiani S, Librizzi L, Hernandez A, Murphy RC, Constantin G, De Curtis M, Folco G, Sala A: Cysteinyl-leukotrienes receptor activation in brain inflammatory reactions and cerebral edema formation: a role for transcellular biosynthesis of cysteinyl-leukotrienes. FASEB J 2004, 18:842–844
46. Uzonyi B, Lotzer K, Jahn S, Kramer C, Hildner M, Bretschneider E, Radke D, Beer M, Vollandt R, Evans JF, Funk CD, Habenicht AJ: Cysteinyl leukotriene 2 receptor and protease-activated receptor 1 activate strongly correlated early genes in human endothelial cells. Proc Natl Acad Sci USA 2006, 103:6326–6331
47. Yan SF, Fujita T, Lu J, Okada K, Shan Zou Y, Mackman N, Pinsky DJ, Stern DM: Egr-1, a master switch coordinating upregulation of divergent gene families underlying ischemic stress. (Erratum in: Nat Med 2001, 7:509). Nat Med 2000, 6:1355–1361
48. Figueroa DJ, Breyer RM, Defoe SK, Kargman S, Daugherty BL, Waldburger K, Liu Q, Clements M, Zeng Z, O'Neill GP, Jones TR, Lynch KR, Austin CP, Evans JF: Expression of the cysteinyl leukotriene 1 receptor in normal human lung and peripheral blood leukocytes. Am J Respir Crit Care Med 2001, 163:226–233
49. Adamek A, Jung S, Dienesch C, Laser M, Ertl G, Bauersachs J, Frantz S: Role of 5-lipoxygenase in myocardial ischemia-reperfusion injury in mice. Eur J Pharmacol 2007, 57:51–54
50. Hu H, Chen G, Zhang JM, Zhang WP, Zhang L, Ge QF, Yao HT, Ding W, Chen Z, Wei EQ: Distribution of cysteinyl leukotriene receptor 2 in human traumatic brain injury and brain tumors. Acta Pharmacol Sin 2005, 26:685–690
51. Crow MT, Mani K, Nam Y-J, Kitsis RN: The mitochondrial death pathway and cardiac myocyte apoptosis. Circ Res 2004, 95:957–970
52. Eefting F, Rensing B, Wigman J, Pannekoek WJ, Liu WM, Cramer MJ, Lips DJ, Doevendans PA: Role of apoptosis in reperfusion injury. Cardiovasc Res 2004, 61:414–426
53. Duilio C, Ambrosio G, Kuppusamy P, DiPaula A, Becker LC, Zweier JL: Neutrophils are primary source of O2 radicals during reperfusion after prolonged myocardial ischemia. Am J Physiol 2001, 280:H2649–H2657

Platelet-Activating Factor Production in the Spinal Cord of Experimental Allergic Encephalomyelitis Mice via the Group IVA Cytosolic Phospholipase A_2-Lyso-PAFAT Axis[1]

Yasuyuki Kihara,* Keisuke Yanagida,* Kayo Masago,* Yoshihiro Kita,* Daisuke Hishikawa,* Hideo Shindou,* Satoshi Ishii,*† and Takao Shimizu[2]*

Platelet-activating factor (PAF; 1-*O*-alkyl-2-acetyl-*sn*-glycero-3-phosphocholine) plays a critical role in inflammatory disorders including experimental allergic encephalomyelitis (EAE), an animal model for multiple sclerosis (MS). Although PAF accumulation in the spinal cord (SC) of EAE mice and cerebrospinal fluid of MS patients has been reported, little is known about the metabolic processing of PAF in these diseases. In this study, we demonstrate that the activities of phospholipase A_2 (PLA_2) and acetyl-CoA:lyso-PAF acetyltransferase (LysoPAFAT) are elevated in the SC of EAE mice on a C57BL/6 genetic background compared with those of naive mice and correlate with disease severity. Correspondingly, levels of groups IVA, IVB, and IVF cytosolic PLA_2s, group V secretory PLA_2, and LysoPAFAT transcripts are up-regulated in the SC of EAE mice. PAF acetylhydrolase activity is unchanged during the disease course. In addition, we show that LysoPAFAT mRNA and protein are predominantly expressed in microglia. Considering the substrate specificity and involvement of PAF production, group IVA cytosolic PLA_2 is likely to be responsible for the increased PLA_2 activity. These data suggest that PAF accumulation in the SC of EAE mice is profoundly dependent on the group IVA cytosolic PLA_2/LysoPAFAT axis present in the infiltrating macrophages and activated microglia. ***The Journal of Immunology*****, 2008, 181: 5008–5014.**

Platelet-activating factor (PAF[3]; 1-*O*-alkyl-2-acetyl-*sn*-glycero-3-phosphocholine), a potent proinflammatory lipid mediator (1), is believed to be synthesized via two distinct pathways, the de novo and remodeling pathways (Ref. 2 and see Fig. 1). The latter pathway is primarily involved in the synthesis of PAF by stimulated inflammatory cells such as murine peritoneal cells (3, 4) and human granulocytes (5). The initiation of the remodeling pathway requires membrane phospholipid hydrolysis by phospholipase A_2s (PLA_2; EC 3.1.1.4) that supply lyso-PAF, a precursor of PAF. Acetyl-CoA:lyso-PAF acetyltransferase (LysoPAFAT; EC 2.3.1.67) converts lyso-PAF into PAF. PAF activates the PAF receptor (PAFR), a member of the superfamily of G protein-coupled receptors (6), and elicits a variety of biological responses (1). PAF is rapidly degraded by PAF acetylhydrolases (PAF-AH; EC 3.1.1.47) that cleave the acetyl group at the *sn*-2 position to reform lyso-PAF (7).

PLA_2 are classified into three groups: group VI calcium-independent PLA_2s (iPLA_2s), secretory PLA_2s (sPLA_2s), and group IV cytosolic PLA_2s (cPLA_2) (8). Group IVA cPLA_2 preferentially liberates arachidonic acid from 2-arachidonoyl-phospholipids (8, 9). The released arachidonic acids are in turn converted into PGs and leukotrienes via the arachidonic acid cascade (10). It is thought that group VI iPLA_2 and some types of sPLA_2s have the potential to initiate the arachidonic acid cascade, even though these enzymes lack significant substrate specificity (8). Group IVA cPLA_2 is also essential for producing PAF, since PAF synthesis is significantly diminished in calcium ionophore-stimulated macrophages derived from group IVA cPLA_2-deficient mice as compared with those from wild-type mice (11). Recently, our group has successfully overcome the long-standing challenges of cloning and identifying LysoPAFAT (12), a critical enzyme that produces PAF. We termed the enzyme LsoPAFAT/LPCAT2 (lysophosphatidylcholine acyltransferase 2) (12). We have demonstrated that murine macrophages and neutrophils express LysoPAFAT/LPCAT2 mRNA and possess a LysoPAFAT activity (3, 12). Furthermore, LysoPAFAT/LPCAT2 mRNA is induced by the ligands for TLRs 4 and 9 in murine macrophages (12). These results imply that LysoPAFAT plays a crucial role in the enhanced PAF production in inflammatory disorders.

Multiple sclerosis (MS) is considered to be a $CD4^+$ T cell-mediated autoimmune disease and is characterized by inflammation and demyelination in the CNS (13). The mechanism of MS,

*Department of Biochemistry and Molecular Biology, Faculty of Medicine, University of Tokyo, Tokyo, Japan; and †Precursory Research for Embryonic Science and Technology of Japan Science and Technology Agency, Tokyo, Japan

Received for publication October 9, 2007. Accepted for publication July 21, 2008.

The costs of publication of this article were defrayed in part by the payment of page charges. This article must therefore be hereby marked *advertisement* in accordance with 18 U.S.C. Section 1734 solely to indicate this fact.

[1] This work was supported, in part, by Grants-in-Aid from the Ministry of Education, Science, Culture, Sports and Technology of Japan (to T. S. and S. I.), a grant to the Respiratory Failure Research Group from the Ministry of Health, Labour and Welfare, Japan (to S. I.), Grants-in-Aid for Comprehensive Research on Aging and Health from the Ministry of Health, Labour and Welfare, Japan (to S. I.), the Kato Memorial Trust for Nambyo Research (to S. I.), and the Japanese Society for the Promotion of Science (research fellowships to Y.Ki., D.H., and K.Y.). H.S., S.I., and T.S. were supported by the Center for NanoBio Integration (University of Tokyo).

[2] Address correspondence and reprint requests to Dr. Takao Shimizu, Department of Biochemistry and Molecular Biology, Faculty of Medicine, University of Tokyo, 7-3-1 Hongo, Bunkyo, Tokyo 113-0033, Japan. E-mail address: tshimizu@m.u-tokyo.ac.jp

[3] Abbreviations used in this paper: PAF, platelet-activating factor; PLA_2, phospholipase A_2; LysoPAFAT, acetyl-CoA:lyso-PAF acetyltransferase; LysoPAFAT/LPCAT2, LysoPAFAT/lysophosphatidylcholine acyltransferase 2; lyso-PAF, 1-*O*-alkyl-*sn*-glycero-3-phosphocholine; PAFR, PAF receptor; PAF-AH, PAF acetylhydrolase; PC, phosphatidylcholine; iPLA_2, calcium-independent PLA_2; sPLA_2, secretory PLA_2; cPLA_2, cytosolic PLA_2; MS, multiple sclerosis; EAE, experimental allergic encephalomyelitis; MOG, myelin oligodendrocyte glycoprotein; SC, spinal cord; ESI-MS/MS, electrospray ionization-tandem mass spectrometry; LPCAT1, lysophosphatidylcholine acyltransferase 1; APMSF, amidinophenylmethanesulfonyl fluoride; GFAP, glial fibrillary acidic protein.

however, remains obscure because of limited access to the CNS at various phases of MS. An animal model, experimental allergic encephalomyelitis (EAE), is indispensable for a better understanding of MS pathology (14). Howat et al. (15) suggested an involvement of PAF in EAE for the first time. We have found that PAFR-KO mice immunized with myelin oligodendrocyte glycoprotein (MOG) peptide 35–55 (MOG_{35-55}) show less severe symptoms than wild-type mice (16). Group IVA $cPLA_2$ deficiency protects mice from EAE pathology (17). We also have reported that there is a correlation between the PAF level in the spinal cord (SC) and EAE symptoms (16), which is consistent with PAF levels in the cerebrospinal fluid of relapsing-remitting MS patients (18). In the SC of EAE mice, PAF seems to exist in the nanomolar range, which is adequate to provoke biological responses through the PAFR (6). Moreover, the level of PAFR transcript is up-regulated in MS lesions (19) and the CNS of EAE-induced SJL and C57BL/6 mice (16, 20). The elevated levels of both PAF and PAFR transcripts probably worsen the MS/EAE pathology. EAE, as an animal model of MS, is useful for understanding the roles of PAF in MS (14), since studies on PAF in MS lesions are in accordance with those in EAE lesions (16, 18–20). However, the metabolic processing of PAF and involvement of LysoPAFAT/LPCAT2 in EAE pathology are largely unknown. In the present study, we have induced EAE in C57BL/6 mice with the MOG_{35-55} peptide and revealed that PAF accumulation in SCs of EAE mice is dependent on the up-regulation of the expression and activities of both group IVA $cPLA_2$ and LysoPAFAT. This is the first report suggesting the involvement of LysoPAFAT/LPCAT2 in the disease models.

Materials and Methods

Induction of EAE

EAE was induced in 8-wk-old C57BL/6 female mice. The maintenance of the facility and the use of animals were in full compliance with the University of Tokyo Ethics Committee for Animal Experiments. MOG_{35-55} (MEVGWYRSPFSRVVHLYRNGK), corresponding to the fragment of mouse MOG from aa 35–55, was synthesized by Sigma-Aldrich. Mice were immunized s.c. in the flank with 300 μg of MOG_{35-55} peptide in 0.1 ml of PBS and 0.1 ml of CFA containing 0.4 mg of *Mycobacterium tuberculosis* (H37Ra; Difco Laboratories) on days 0 and 7 and injected i.p. with 250 ng of pertussis toxin (List Biological Laboratories) on days 0 and 2. Mice were scored as follows: 0, no sign; 0.5, mild loss of tail tone; 1.0, complete loss of tail tone; 1.5, mildly impaired righting reflex; 2.0, abnormal gait and/or impaired righting reflex; 2.5, hind limb paresis; 3.0, hind limb paralysis; 3.5, hind limb paralysis with hind body paresis; 4.0, hind and fore limb paralysis; 4.5, moribund; and 5.0, death. To understand the EAE pathology, we divided the disease course into induction, acute, and chronic phases in accordance with the clinical symptoms as previously described (Ref. 16 and Fig. 2*A*).

Quantification of PAF

PAF and eicosanoid levels were estimated simultaneously as previously described (21, 22). The results of the eicosanoid levels will be published elsewhere (Y. Kihara, S. Ishii, Y. Kita, S. Uematsu, S. Akira, and T. Shimizu, unpublished data). SCs of naive mice and EAE mice were removed on days 12, 19, and 32, frozen immediately with liquid nitrogen, and stored at −80°C until use. The frozen tissues (~100 mg) were powdered with an SK-100 mill (Tokken), and lipids were extracted for 60 min at 4°C with methanol containing deuterium-labeled 16:0 PAF (Cayman Chemical) as an internal standard. The extracts were loaded onto Oasis HLB cartridges (30 mg; Waters) preloaded with methanol and 0.03% (v/v) formic acid/H_2O. The cartridges were washed with 0.03% formic acid/H_2O, 15% (v/v) ethanol, and petroleum ether. Lipids were extracted with 100% methanol and PAF levels were quantified by reversed-phase HPLC electrospray ionization (ESI)-tandem mass spectrometry (MS/MS) as described previously (21, 22).

Quantitative real-time PCR

On days 11–12, 18–19, and 30–31, naive and EAE mice were anesthetized with urethane (1.5 g/kg of body; Sigma-Aldrich) and intracardially perfused with 10 ml of ice-cold PBS. The SCs were removed and total RNA was isolated using an RNeasy Mini Kit (Qiagen). The purity and integrity of total RNA were determined by the absorbance at $A_{260/280}$ and gel electrophoresis, respectively. One microgram of total RNA was reverse-transcribed using SuperScript II (Invitrogen Life Technologies) according to the manufacturer's instructions. The RT^2 Profiler PCR Array System for PLA_2 (groups IVA, IVB, IVC, IVD, IVE, and IVF $cPLA_2$s, groups V and X $sPLA_2$s, and group VI $iPLA_2$) was purchased from SuperArray, and quantitative RT-PCR for these PLA_2 mRNAs was performed with a 7500 Fast Real-Time PCR System (Applied Biosystems). The relative abundance of PLA_2 mRNA levels in EAE mice compared with naive mice was calculated by the comparative cycle threshold method using hypoxanthine phosphoribosyltransferase as a normalization control. Quantification of LysoPAFAT, lysophosphatidylcholine acyltransferase 1 (LPCAT1), and β-actin mRNA levels was performed with LightCycler FastStart DNA Master SYBR Green I (Roche) as previously described (12, 23). Results were quantified by using standard curves derived from SCs in the acute phase of EAE.

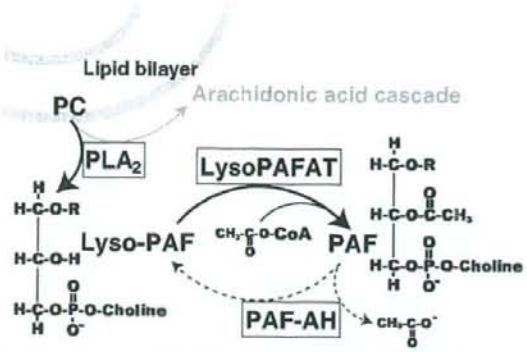

FIGURE 1. PAF production in the remodeling pathway (bold arrow) and degradation pathway (dotted arrow).

Sample preparation for enzyme assays and Western blotting

The SCs of naive mice and EAE mice on days 12, 19, and 34 were removed following perfusion, frozen immediately with liquid nitrogen, and stored at −80°C until use. The tissues (~100 mg) were homogenized with a Physcotoron homogenizer (Microtec) in 500 μl of buffer A (100 mM Tris-HCl (pH 7.4) containing 10.26% sucrose, 20 μM amidinophenylmethanesulfonyl fluoride (APMSF), 5 mM 2-ME, and 1 × Complete Protease Inhibitor Mixture (Roche)). The homogenate was centrifuged at 9,000 × g for 10 min at 4°C and the resulting supernatant was centrifuged at 100,000 × g for 60 min at 4°C. The pellet was resuspended in buffer B (20 mM Tris-HCl (pH 7.4) containing 20 μM APMSF, 5 mM 2-ME, and EDTA-free 1 × Complete Protease Inhibitor Mixture) and stored at −80°C until use. Protein concentrations were determined by the Bradford method using a protein assay solution (Bio-Rad) and BSA (fraction V, fatty acid-free; Sigma-Aldrich) as a standard.

PLA_2 assay

PLA_2 activity was measured by Dole's method with some modifications (24). Briefly, 5 μg of protein (100,000 × g supernatant) was incubated at 37°C for 30 min in a total volume of 0.25 ml of assay buffer (100 mM HEPES-NaOH (pH 7.4) 1 mg/ml BSA, 4 mM $CaCl_2$, and 1 mM DTT) containing mixed micelles (4 μM Triton X-100 and 2 μM 1-palmitoyl-2-[^{14}C]arachidonoyl-phosphatidylcholine (PC) (1.961 GBq/mmol, GE Healthcare BioSciences). The reaction was terminated by adding 1.25 ml of Dole's reagent (isopropanol:*n*-heptane:sulfuric acid, 78:20:2), followed by the sequential addition of 0.75 ml of *n*-heptane and 0.5 ml of water. After centrifugation, an aliquot (0.8 ml) of the upper layer was mixed with 120–150 mg of silica gel, which had been preincubated with 0.75 ml of *n*-heptane. The radioactivity of an aliquot (0.8 ml) was estimated using an LS6500 liquid scintillation counter (Beckman Coulter) in the presence of 1 ml of Microscinti-0 (PerkinElmer).

LysoPAFAT assay

LysoPAFAT activity was measured according to the method of Kume et al. (4, 12, 25), with some modifications. Briefly, 5 μg of protein (100,000 ×

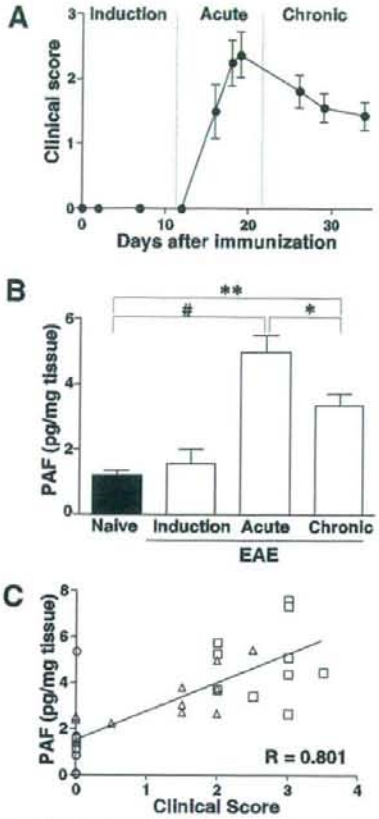

FIGURE 2. Clinical course and PAF levels during EAE. *A*, C57BL/6 female mice were immunized with the MOG_{35-55} peptide. Data are the mean clinical scores ± SEM of eight animals. *B*, PAF levels were determined in SCs of naive mice and EAE mice in the induction, acute, and chronic phases (n = 10 animals). Data represent means ± SEM. #, $p < 0.001$; **, $p < 0.01$; and *, $p < 0.05$ by ANOVA with the Tukey-Kramer test. *C*, PAF levels of naive (●) and EAE mice in the induction (○), acute (□), and chronic (△) phases are positively correlated with the clinical scores ($p < 0.0001$ by the Spearman rank correlation test). Each data point represents the result from a single animal.

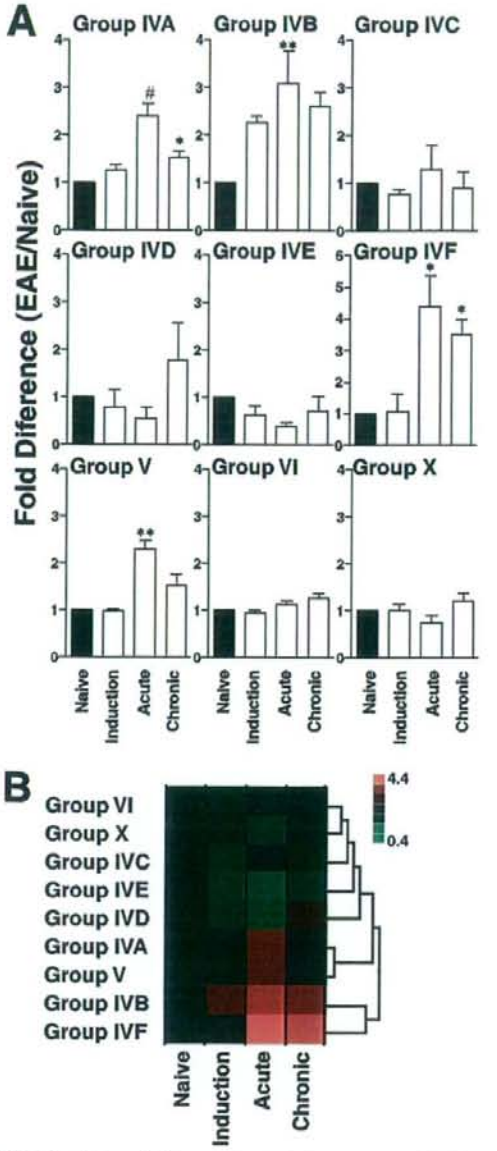

FIGURE 3. PLA_2 mRNA expression in SCs of naive and EAE mice. *A*, Expression of PLA_2 transcripts was quantified by real-time PCR in SCs of naive mice and EAE mice in the induction, acute, and chronic phases (n = 6, 5, 6, and 5 animals, respectively). The relative abundance of PLA_2 mRNA levels in EAE mice compared with naive mice is shown. Data represent means ± SEM. #, $p < 0.001$; **, $p < 0.01$; and *, $p < 0.05$ compared with naive mice by the Kruskal-Wallis test with Dunn's post hoc test. *B*, The relationships among PLA_2 mRNA levels were evaluated by cluster analysis using JMP6 software (Hulinks). The relative expression levels shown in *A* are divided into seven parts and colored from red to green.

g pellet) was incubated at 37°C for 10 min in a total volume of 0.1 ml of reaction mixture (buffer B containing 2 mM $CaCl_2$, 1 mg/ml PC (Sigma-Aldrich), and 100 μM [^{3}H]acetyl-CoA (1.11 GBq/mmol; GE Healthcare BioSciences)) with or without 20 μM lyso-PAF (Cayman Chemical). Subsequently, 122 μl of ice-cold methanol was added to terminate the reaction. The product was bound to 6 mg of C8 resin (Millipore), washed eight times with 55% (v/v) methanol in 20 mM Tris-HCl (pH 7.4), and eluted with 100% methanol. After drying at 50°C for 2 h, the radioactivity was determined using a TopCount microplate scintillation counter (PerkinElmer) in the presence of 200 μl of Microscinti-0. LysoPAFAT activity was calculated by subtracting the radioactivity obtained without lyso-PAF from that obtained with lyso-PAF.

PAF-AH assay

PAF-AH activity was evaluated under the same conditions as reported previously, with minor modifications (26, 27). Briefly, 10 μg of protein (100,000 × g supernatant) was incubated at 37 °C for 30 min in a total volume of 0.25 ml of assay buffer (50 mM Tris-HCl (pH 7.4), 5 mM EDTA, 5 mM 2-ME, and 100 μM [*acetyl*-^{3}H]PAF (85 MBq/mmol; PerkinElmer)). The reaction was stopped by adding 2.5 ml of chloroform/methanol (4:1, v/v), followed by 0.25 ml of water. The radioactivity of an aliquot (0.6 ml) of each water phase was measured with 2 ml of the liquid scintillation mixture, Atomlight (PerkinElmer), to determine the amount of acetyl groups liberated from PAF.

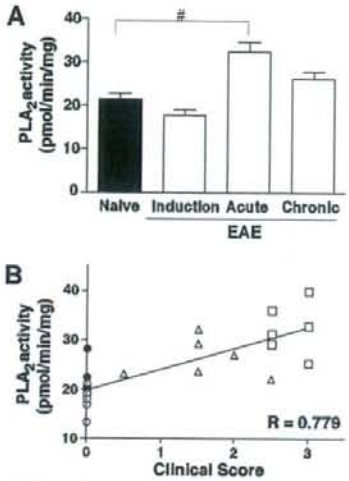

FIGURE 4. PLA_2 activity in SCs of naive and EAE mice. *A*, PLA_2 activity in SCs of naive mice and EAE mice in the induction, acute, and chronic phases ($n = 6$ animals) was measured using mixed micelles containing 1-palmitoyl-2-[^{14}C]arachidonoyl-PC and Triton X-100 in the presence of Ca^{2+} and DTT. Data represent means ± SEM. #, $p < 0.001$ by ANOVA with the Tukey-Kramer test. *B*, PLA_2 activity in naive (●) and EAE mice in the induction (○), acute (□), and chronic (△) phases is positively correlated with the clinical score ($p < 0.0001$ by the Spearman rank correlation test). Each data point represents the result from a single animal.

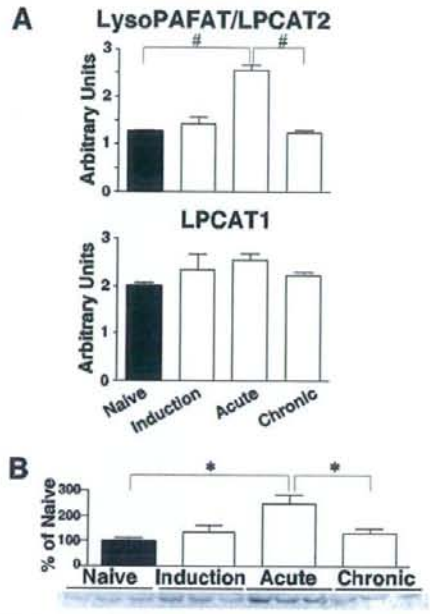

FIGURE 5. LysoPAFAT/LPCAT2 expression in SCs of naive and EAE mice. Expression levels of LysoPAFAT/LPCAT2 and LPCAT1 mRNAs (*A*) and LysoPAFAT/LPCAT2 proteins (*B*) were quantified by real-time PCR and Western blotting with densitometry, respectively, in SCs of naive mice and EAE mice in the induction, acute, and chronic phases ($n = 6$ animals). A representative blot from two independent experiments is shown for LysoPAFAT ($n = 3$ animals). Data represent means ± SEM. #, $p < 0.001$ and *, $p < 0.05$ by ANOVA with the Tukey-Kramer test.

Western blotting

Ten micrograms of protein was resolved by 10% SDS-PAGE and transferred to a Hybond ECL nitrocellulose membrane (GE Healthcare Bio-Sciences). The membrane was blocked with 5% skim milk and incubated with anti-LysoPAFAT antiserum (Immuno-Biological Laboratories). After washing, the membranes were incubated with HRP-linked anti-rabbit IgG (GE Healthcare BioSciences), washed, and then exposed to the Western blotting detection reagents (GE Healthcare BioSciences). The membranes were scanned with a LAS-4000 luminescent image analyzer (Fuji film).

Primary culture

Primary young cortical neurons were prepared from C57BL/6 mouse brains on embryonic day 13 as previously described (28, 29). Primary astrocytes and microglia were obtained from cerebral hemispheres of C57BL/6 mouse brains on postnatal day 1, as previously described, with minor modifications (28–30). Briefly, after a 14-day culture period, astrocytes were purified by two passages. Microglia was prepared as a floating cell suspension and transferred to culture dishes. Unattached cells were removed before isolating total RNA. The purities of astrocytes and microglia were estimated to be >90% and >99%, respectively, by immunostaining for glial fibrillary acidic protein (GFAP) and Iba1. Total RNA (1 μg) was reverse-transcribed as described above.

$CD4^+$ and $CD8^+$ T cells were obtained from spleens of C57BL/6 mice using a MACS magnetic cell separation system (Miltenyi Biotec). The purities of $CD4^+$ and $CD8^+$ T cells were estimated to be >90% by flow cytometry (Beckman Coulter). T cells were stimulated with or without anti-CD3e Ab (BD Biosciences) for 24 h, followed by reverse transcription of total RNA (100 ng) as described above.

Statistical analysis

Results are expressed as means ± SEM. Data were analyzed statistically by means of ANOVA with the Tukey-Kramer post hoc test, the Kruskal-Wallis test with Dunn's post hoc test, or the Spearman rank correlation test as appropriate, using GraphPad PRISM software. Values of $p < 0.05$ were considered to be statistically significant. Cluster analysis was performed using JMP6 software (Hulinks).

Results

Elevation of PAF levels in SCs of EAE mice

C57BL/6 female mice were immunized with MOG_{35-55} and clinical symptoms were monitored (Fig. 2*A*). All mice developed EAE and the mean maximal clinical score was 2.6 ± 0.16 ($n = 8$ animals). To confirm our previous report, PAF levels in SCs were measured by HPLC-ESI-MS/MS. The SCs were collected from naive mice and immunized mice in the induction, acute, and chronic phases of EAE (Fig. 2*A*). PAF levels were significantly elevated in the acute phase (Fig. 2*B*) and positively correlated with the clinical score ($p < 0.0001$; Fig. 2*C*). Thus, the fluctuation in PAF levels during the disease course was reproduced (16). These results demonstrate that the metabolism of PAF (Fig. 1) in the SC was perturbed by the pathogenesis of EAE. Therefore, we determined the enzymes that synthesize and degrade PAF using EAE mice.

Up-regulation of PLA_2 mRNA expression and activity in SCs of EAE mice

The various PLA_2 (groups IVA, IVB, IVC, IVD, IVE, and IVF $cPLA_2$s, groups V and X $sPLA_2$s, and group VI $iPLA_2$) mRNA levels were determined by quantitative RT-PCR to elucidate the effects of PLA_2s on PAF production. Group IVA $cPLA_2$ and group V $sPLA_2$ mRNA levels were elevated in the acute phase of EAE and decreased in the chronic phase to a level that was still higher than that in naive mice (Fig. 3*A*). The relationships among the mRNA levels were evaluated by cluster analysis that distinguished group IVA $cPLA_2$ and group V $sPLA_2$ from other PLA_2s (Fig. 3*B*). In addition, the poorly characterized groups IVB and IVF

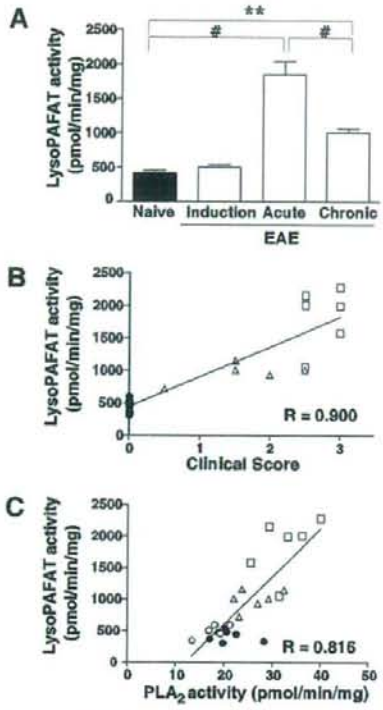

FIGURE 6. LysoPAFAT activity in SCs of naive and EAE mice. *A*, LysoPAFAT activity in SCs of naive mice and EAE mice in the induction, acute, and chronic phases ($n = 6$ animals) was measured as described in *Materials and Methods*. Data represent means ± SEM. #, $p < 0.001$ and **, $p < 0.01$ by ANOVA with the Tukey-Kramer test. *B* and *C*, LysoPAFAT activity in SCs of naive (●) and EAE mice in the induction (○), acute (□), and chronic (△) phases is positively correlated with the clinical score (*B*; $p < 0.0001$ by the Spearman rank correlation test) and PLA_2 activity (*C*; $p < 0.0001$). Each data point represents the results from a single animal.

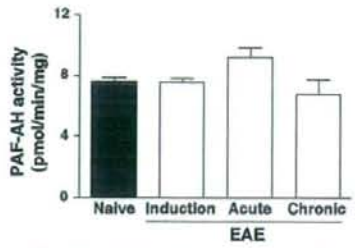

FIGURE 7. PAF-AH activity in SCs of naive and EAE mice. PAF-AH activity in SCs of naive mice and EAE mice in the induction, acute, and chronic phases ($n = 6$ animals) was measured as described in *Materials and Methods*. Data represent means ± SEM.

$cPLA_2$s were up-regulated and clustered together (Fig. 3, *A* and *B*). PLA_2 activity was measured using 1-palmitoyl-2-[^{14}C]arachidonoyl-PC as a substrate with Ca^{2+} and DTT. The enzyme activity increased with the progression of EAE pathology ($p < 0.001$; Fig. 4*A*) and correlated significantly with the clinical score ($p < 0.0001$; Fig. 4B). These results suggest that PAF accumulation in SCs of EAE mice may be due to an up-regulation of PLA_2 and lysoPAFAT (see below).

Enhancement of LysoPAFAT/LPCAT2 expression and activity in SCs of EAE mice

To examine the involvement of LysoPAFAT/LPCAT2, expression levels of the transcripts and proteins were examined in SCs of naive and EAE mice by quantitative RT-PCR and Western blotting, respectively. LysoPAFAT/LPCAT2 transcripts and proteins were elevated in the acute phase and then declined in the chronic phase of EAE (Fig. 5). In contrast, mRNA expression level of the homologous enzyme LPCAT1 was unaltered during the disease course (Fig. 5). In agreement with these observations, the enzyme activities in the acute and chronic phases were higher than those of naive mice ($p < 0.001$; Fig. 6*A*). We found a significantly positive correlation between the clinical score and the LysoPAFAT activity ($p < 0.0001$; Fig. 6*B*). Furthermore, LysoPAFAT activity was positively correlated with PLA_2 activity ($p < 0.001$; Fig. 6*C*). These results suggest that PAF accumulation in SCs of EAE mice is caused by the enhancement of LysoPAFAT/LPCAT2 expression and the corresponding increase in LysoPAFAT activity.

Unaltered basal PAF-AH activity in SCs of EAE mice

We investigated whether PAF-AH affected the accumulation of PAF in SCs of EAE mice. Although PAF-AH activity appeared to be slightly increased in the acute phase of EAE, the enzyme activity did not change significantly during the disease course (Fig. 7). PAF-AH activity did not correlate with the clinical score, PLA_2 activity, or LysoPAFAT activity (data not shown). Thus, PAF accumulation in SCs of EAE mice may be independent of the PAF degradation system.

LysoPAFAT/LPCAT2 expression in primary cultured murine microglia and astrocytes

We previously demonstrated LysoPAFAT/LPCAT2 mRNA expression in murine brain, macrophages, and neutrophils (12). Its expression was determined by RT-PCR and Western blotting in primary cultured murine neurons, astrocytes, microglia (Fig. 8), $CD4^+$ T cells, and $CD8^+$ T cells (data not shown). We found that LysoPAFAT/LPCAT2 mRNA was expressed in microglia and astrocytes, but not in neurons (Fig. 8*A*). The levels of LysoPAFAT/LPCAT2 transcripts were very low in both T cell subsets, with or without anti-CD3ε Ab stimulation for 24 h (data not shown). LysoPAFAT/LPCAT2 protein expression was observed in microglia, but not in astrocytes (Fig. 8*B*). These results suggest that PAF may

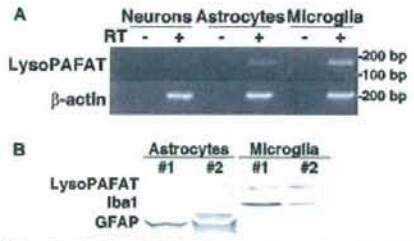

FIGURE 8. LysoPAFAT/LPCAT2 expression in the primary cultured cells of the murine CNS. *A*, LysoPAFAT/LPCAT2 and β-actin mRNA expression in primary cultured neurons, astrocytes, and microglia was determined by RT-PCR. The expected PCR products for LysoPAFAT and β-actin were 167 and 197 bp, respectively. *B*, Expression of LysoPAFAT/LPCAT2, Iba1, and GFAP in primary cultured astrocytes and microglia was determined by Western blotting. Each lane represents cells purified from an individual experiment.

be produced by activated microglia and infiltrating macrophages in SCs of EAE mice.

Discussion

In the present study, we have assessed the metabolic processing of PAF in SCs of naive and EAE mice to explain the enhanced PAF production in EAE mice. In general, accumulation of PAF can be accounted for by the up-regulation of the production system in the remodeling pathway and/or the down-regulation of the degradation system. We have demonstrated that the PAF production system is increased and the degradation system is unchanged in SCs during EAE.

The PAF production system in the remodeling pathway consists of two steps. The first step is production of the PAF precursor lyso-PAF by PLA_2s that hydrolyze the *sn*-2 acyl chain of PC (9) (Fig. 1). Several lines of evidence have suggested that group IVA $cPLA_2$, groups IIA and V $sPLA_2$s, and group VI $iPLA_2$ mRNAs are expressed in the SC of the naive rat (31, 32). In agreement with these studies, we have found that SCs of C57BL/6 mice express these PLA_2 mRNAs, with the exception of group IIA $sPLA_2$ (Fig. 3), which is absent in this mouse strain (33). Because the groups IVA, IVB, and IVF $cPLA_2$s and group V $sPLA_2$ mRNA levels are elevated in the acute phase of EAE (Fig. 3), lipid mediators produced by these four PLA_2s presumably participate in the pathogenesis of EAE. Although little is known about the functions of groups IVB and IVF $cPLA_2$s, it is generally accepted that group IVA $cPLA_2$ and group V $sPLA_2$ stimulate the arachidonic acid cascade (33). Indeed, hierarchical cluster analysis demonstrates the functional analogy of these PLA_2s in EAE pathology (Fig. 3*B*). EAE is not completely ameliorated in PAFR-KO mice (16), whereas group IVA $cPLA_2$ deficiency or treatments with PLA_2 inhibitors protect mice from the EAE pathology (17, 34). Eicosanoid levels were quantified simultaneously and we found that PGE_2 levels were dramatically changed during the disease course (Y. Kihara, S. Ishii, Y. Kita, S. Uematsu, S. Akira, and T. Shimizu, unpublished data). These data suggest that, not only PAF, but also eicosanoids downstream of PLA_2 are critical for the EAE pathology. We have demonstrated the elevation of PLA_2 activity in the acute phase of EAE using 1-palmitoyl-2-[^{14}C]arachidonoyl-PC as a substrate in the presence of Ca^{2+} and DTT (Fig. 4). Since this assay condition is optimized for group IV $cPLA_2$s (35), the elevated PLA_2 activity in the acute phase of EAE may be derived from groups IVA, IVB, and/or IVF $cPLA_2$s. However, groups IVB and IVF $cPLA_2$s have lower PLA_2 activity than group IVA $cPLA_2$ under the present assay conditions (24, 36, 37). Thus, group IVA $cPLA_2$ may be deeply involved in the up-regulation of PLA_2 activity in SCs of EAE mice. Additionally, group IVA $cPLA_2$ is essential for producing PAF, since PAF synthesis is significantly diminished in calcium ionophore-stimulated group IVA $cPLA_2$-deficient macrophages (11). These results suggest that the PAF precursor lyso-PAF is supplied primarily by group IVA $cPLA_2$ during EAE. Because Cunningham et al. (38) reported that $sPLA_2$ activity was up-regulated in urine of EAE rats and MS patients, it may play roles in the EAE pathology. In addition, Bernatchez et al. (39) reported that group V $sPLA_2$ is involved in the PAF production in endothelial cells. Further studies are needed to clarify the roles of group V $sPLA_2$ in EAE lesions.

The second step of the PAF production system is acetylation of lyso-PAF to form PAF by the action of LysoPAFAT, which is critical for the stimulus-dependent formation of PAF (2–4, 12). We have previously shown that LysoPAFAT/LPCAT2 mRNA is expressed in brain, macrophages, and neutrophils (12). Likewise, we have demonstrated the constitutive expression and activity of LysoPAFAT in the SC of naive mice (Figs. 5 and 6). Since LysoPAFAT/LPCAT2 expression is mainly detected in primary cultured microglia by RT-PCR and Western blotting (Fig. 8), microglia may contribute to the production of PAF in the CNS of naive mice for maintaining brain homeostasis (Fig. 9, *left*). A number of inflammatory cells, such as T cells and macrophages, infiltrate the CNS through the broken blood-brain barrier in EAE mice. Furthermore, microglia and astrocytes are activated by cytokines produced by the infiltrating cells (40, 41). The expression and activity of LysoPAFAT were significantly elevated in SCs of EAE mice as compared with those of naive mice (Figs. 5 and 6). Because LysoPAFAT/LPCAT2 is an inducible protein, its expression might be strongly up-regulated in infiltrating macrophages and activated microglia (Fig. 9, *right*). We also have shown that LysoPAFAT activity is correlated with PLA_2 activity (Fig. 6*C*). Kalyvas and David (34) have reported that group IVA $cPLA_2$ is expressed in $CD11b^+$ cells from mice with severe symptoms of EAE. Hence, group IVA $cPLA_2$ and LysoPAFAT appear to be coexpressed in the same cells, such as macrophages/microglia, and to function coordinately in PAF synthesis. In contrast, LysoPAFAT/LPCAT2 mRNA was undetected in T cells stimulation with or without anti-CD3ε Ab for 24 h (data not shown). These results are in accord with previous reports demonstrating that LysoPAFAT activity is present in macrophages (4, 12), but not in T cells (42). The results are also consistent with our previous report that PAF plays a dominant role in the chronic phase of EAE through the activation of macrophages/microglia (16). Taken together, LysoPAFAT induced in macrophages/microglia plays a crucial role in PAF production in EAE pathology (Fig. 9, *right*).

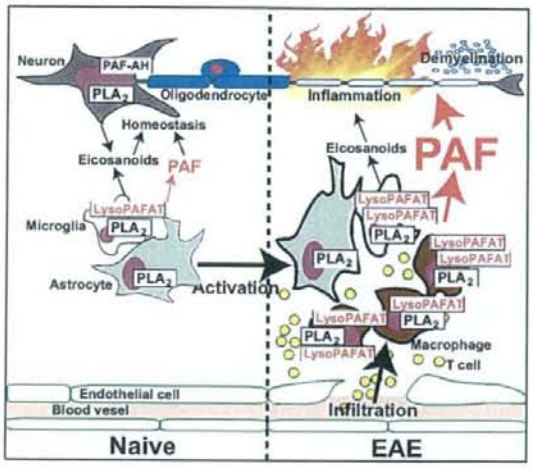

FIGURE 9. Models for PAF production in the CNS of naive mice and EAE mice. *Left*, In the CNS of naive mice, constant levels of PAF produced by microglia and astrocytes may contributes to the maintenance of CNS homeostasis. *Right*, In the CNS of EAE mice, the blood-brain barrier has been broken and inflammatory cells, such as T cells and macrophages, have infiltrated the CNS. LysoPAFAT is induced in activated microglia. Thus, robust PAF production is probably dependent on both LysoPAFAT and group IVA $cPLA_2$ coexpressed in activated macrophages and microglia.

We have measured PAF-AH activity in SCs of naive and EAE mice (Fig. 7) and found that PAF-AH activity is unchanged during the disease course of EAE. Thus, PAF may accumulate in SCs of EAE mice independently of the PAF degradation system.

Our results show that the enzyme activities in the remodeling pathway of PAF synthesis are elevated in SCs of EAE mice due to

up-regulation of group IVA cPLA$_2$ and LysoPAFAT/LPCAT2 present in macrophages and microglia (Fig. 9). Development of LysoPAFAT inhibitors may be therapeutically beneficial for the treatment of MS.

Acknowledgments

We thank Dr. N. Fukushima (Kinki University, Osaka, Japan) for advising us on the primary culturing of neurons and K. Kuniyeda (University of Tokyo, Tokyo, Japan) for valuable suggestions.

Disclosures

The authors have no financial conflict of interest.

References

1. Ishii, S., and T. Shimizu. 2000. Platelet-activating factor (PAF) receptor and genetically engineered PAF receptor mutant mice. *Prog. Lipid Res.* 39: 41–82.
2. Snyder, F. 1995. Platelet-activating factor: the biosynthetic and catabolic enzymes. *Biochem. J.* 305: 689–705.
3. Shindou, H., S. Ishii, N. Uozumi, and T. Shimizu. 2000. Roles of cytosolic phospholipase A$_2$ and platelet-activating factor receptor in the Ca-induced biosynthesis of PAF. *Biochem. Biophys. Res. Commun.* 271: 812–817.
4. Shindou, H., S. Ishii, M. Yamamoto, K. Takeda, S. Akira, and T. Shimizu. 2005. Priming effect of lipopolysaccharide on acetyl-coenzyme A:lyso-platelet-activating factor acetyltransferase is MyD88 and TRIF independent. *J. Immunol.* 175: 1177–1183.
5. Owen, J. S., P. R. Baker, J. T. O'Flaherty, M. J. Thomas, M. P. Samuel, R. E. Wooten, and R. L. Wykle. 2005. Stress-induced platelet-activating factor synthesis in human neutrophils. *Biochim. Biophys. Acta* 1733: 120–129.
6. Honda, Z., M. Nakamura, I. Miki, M. Minami, T. Watanabe, Y. Seyama, H. Okado, H. Toh, K. Ito, T. Miyamoto, and T. Shimizu. 1991. Cloning by functional expression of platelet-activating factor receptor from guinea-pig lung. *Nature* 349: 342–346.
7. Arai, H., H. Koizumi, J. Aoki, and K. Inoue. 2002. Platelet-activating factor acetylhydrolase (PAF-AH). *J. Biochem.* 131: 635–640.
8. Kudo, I., and M. Murakami. 2002. Phospholipase A$_2$ enzymes. *Prostaglandins Other Lipid Mediat.* 68–69: 3–58.
9. Kita, Y., T. Ohto, N. Uozumi, and T. Shimizu. 2006. Biochemical properties and pathophysiological roles of cytosolic phospholipase A2s. *Biochim. Biophys. Acta* 1761: 1317–1322.
10. Funk, C. D. 2001. Prostaglandins and leukotrienes: advances in eicosanoid biology. *Science* 294: 1871–1875.
11. Uozumi, N., K. Kume, T. Nagase, N. Nakatani, S. Ishii, F. Tashiro, Y. Komagata, K. Maki, K. Ikuta, Y. Ouchi, et al. 1997. Role of cytosolic phospholipase A2 in allergic response and parturition. *Nature* 390: 618–622.
12. Shindou, H., D. Hishikawa, H. Nakanishi, T. Harayama, S. Ishii, R. Taguchi, and T. Shimizu. 2007. A single enzyme catalyzes both platelet-activating factor production and membrane biogenesis of inflammatory cells: cloning and characterization of acetyl-CoA:LYSO-PAF acetyltransferase. *J. Biol. Chem.* 282: 6532–6539.
13. Pedotti, R., J. J. De Voss, L. Steinman, and S. J. Galli. 2003. Involvement of both "allergic" and "autoimmune" mechanisms in EAE, MS and other autoimmune diseases. *Trends Immunol.* 24: 479–484.
14. Steinman, L., and S. S. Zamvil. 2006. How to successfully apply animal studies in experimental allergic encephalomyelitis to research on multiple sclerosis. *Ann. Neurol.* 60: 12–21.
15. Howat, D. W., N. Chand, P. Braquet, and D. A. Willoughby. 1989. An investigation into the possible involvement of platelet activating factor in experimental allergic encephalomyelitis in rats. *Agents Actions* 27: 473–476.
16. Kihara, Y., S. Ishii, Y. Kita, A. Toda, A. Shimada, and T. Shimizu. 2005. Dual phase regulation of experimental allergic encephalomyelitis by platelet-activating factor. *J. Exp. Med.* 202: 853–863.
17. Marusic, S., M. W. Leach, J. W. Pelker, M. L. Azoitei, N. Uozumi, J. Cui, M. W. Shen, C. M. DeClercq, J. S. Miyashiro, B. A. Carito, et al. 2005. Cytosolic phospholipase A2 α-deficient mice are resistant to experimental autoimmune encephalomyelitis. *J. Exp. Med.* 202: 841–851.
18. Callea, L., M. Arese, A. Orlandini, C. Bargnani, A. Priori, and F. Bussolino. 1999. Platelet activating factor is elevated in cerebral spinal fluid and plasma of patients with relapsing-remitting multiple sclerosis. *J. Neuroimmunol.* 94: 212–221.
19. Lock, C., G. Hermans, R. Pedotti, A. Brendolan, E. Schadt, H. Garren, A. Langer-Gould, S. Strober, B. Cannella, J. Allard, et al. 2002. Gene-microarray analysis of multiple sclerosis lesions yields new targets validated in autoimmune encephalomyelitis. *Nat. Med.* 8: 500–508.
20. Pedotti, R., J. J. DeVoss, S. Youssef, D. Mitchell, J. Wedemeyer, R. Madanat, H. Garren, P. Fontoura, M. Tsai, S. J. Galli, et al. 2003. Multiple elements of the allergic arm of the immune response modulate autoimmune demyelination. *Proc. Natl. Acad. Sci. USA* 100: 1867–1872.
21. Kita, Y., T. Takahashi, N. Uozumi, L. Nallan, M. H. Gelb, and T. Shimizu. 2005. Pathway-oriented profiling of lipid mediators in macrophages. *Biochem. Biophys. Res. Commun.* 330: 898–906.
22. Kita, Y., T. Takahashi, N. Uozumi, and T. Shimizu. 2005. A multiplex quantitation method for eicosanoids and platelet-activating factor using column-switching reversed-phase liquid chromatography-tandem mass spectrometry. *Anal. Biochem.* 342: 134–143.
23. Nakanishi, H., H. Shindou, D. Hishikawa, T. Harayama, R. Ogasawara, A. Suwabe, R. Taguchi, and T. Shimizu. 2006. Cloning and characterization of mouse lung-type acyl-CoA:lysophosphatidylcholine acyltransferase 1 (LPCAT1): expression in alveolar type II cells and possible involvement in surfactant production. *J. Biol. Chem.* 281: 20140–20147.
24. Ohto, T., N. Uozumi, T. Hirabayashi, and T. Shimizu. 2005. Identification of novel cytosolic phospholipase A$_2$s, murine cPLA$_2$δ, ε, and ζ, which form a gene cluster with cPLA$_2$β. *J. Biol. Chem.* 280: 24576–24583.
25. Kume, K., I. Waga, and T. Shimizu. 1997. Microplate chromatography assay for acetyl-CoA: lysoplatelet-activating factor acetyltransferase. *Anal. Biochem.* 246: 118–122.
26. Hattori, K., M. Hattori, H. Adachi, M. Tsujimoto, H. Arai, and K. Inoue. 1995. Purification and characterization of platelet-activating factor acetylhydrolase II from bovine liver cytosol. *J. Biol. Chem.* 270: 22308–22313.
27. Ohshima, N., S. Ishii, T. Izumi, and T. Shimizu. 2002. Receptor-dependent metabolism of platelet-activating factor in murine macrophages. *J. Biol. Chem.* 277: 9722–9727.
28. Mori, M., M. Aihara, K. Kume, M. Hamanoue, S. Kohsaka, and T. Shimizu. 1996. Predominant expression of platelet-activating factor receptor in the rat brain microglia. *J. Neurosci.* 16: 3590–3600.
29. Aihara, M., S. Ishii, K. Kume, and T. Shimizu. 2000. Interaction between neurone and microglia mediated by platelet-activating factor. *Genes Cells* 5: 397–406.
30. Tabuchi, S., K. Kume, M. Aihara, and T. Shimizu. 2000. Expression of lysophosphatidic acid receptor in rat astrocytes: mitogenic effect and expression of neurotrophic genes. *Neurochem. Res.* 25: 573–582.
31. Lucas, K. K., C. I. Svensson, X. Y. Hua, T. L. Yaksh, and E. A. Dennis. 2005. Spinal phospholipase A2 in inflammatory hyperalgesia: role of group IVA cPLA2. *Br. J. Pharmacol.* 144: 940–952.
32. Svensson, C. I., K. K. Lucas, X. Y. Hua, H. C. Powell, E. A. Dennis, and T. L. Yaksh. 2005. Spinal phospholipase A$_2$ in inflammatory hyperalgesia: role of the small, secretory phospholipase A$_2$. *Neuroscience* 133: 543–553.
33. Murakami, M., and I. Kudo. 2002. Phospholipase A$_2$. *J. Biochem.* 131: 285–292.
34. Kalyvas, A., and S. David. 2004. Cytosolic phospholipase A$_2$ plays a key role in the pathogenesis of multiple sclerosis-like disease. *Neuron* 41: 323–335.
35. Lucas, K. K., and E. A. Dennis. 2005. Distinguishing phospholipase A$_2$ types in biological samples by employing group-specific assays in the presence of inhibitors. *Prostaglandins Other Lipid Mediat.* 77: 235–248.
36. Pickard, R. T., B. A. Strifler, R. M. Kramer, and J. D. Sharp. 1999. Molecular cloning of two new human paralogs of 85-kDa cytosolic phospholipase A$_2$. *J. Biol. Chem.* 274: 8823–8831.
37. Song, C., X. J. Chang, K. M. Bean, M. S. Proia, J. L. Knopf, and R. W. Kriz. 1999. Molecular characterization of cytosolic phospholipase A$_2$-β. *J. Biol. Chem.* 274: 17063–17067.
38. Cunningham, T. J., L. Yao, M. Oetinger, L. Cort, E. P. Blankenhorn, and J. I. Greenstein. 2006. Secreted phospholipase A$_2$ activity in experimental autoimmune encephalomyelitis and multiple sclerosis. *J. Neuroinflammation* 3: 26.
39. Bernatchez, P. N., M. V. Winstead, E. A. Dennis, and M. G. Sirois. 2001. VEGF stimulation of endothelial cell PAF synthesis is mediated by group V 14 kDa secretory phospholipase A$_2$. *Br. J. Pharmacol.* 134: 197–205.
40. Benveniste, E. N. 1997. Role of macrophages/microglia in multiple sclerosis and experimental allergic encephalomyelitis. *J. Mol. Med.* 75: 165–173.
41. Bannerman, P., A. Hahn, A. Soulika, V. Gallo, and D. Pleasure. 2007. Astrogliosis in EAE spinal cord: derivation from radial glia, and relationships to oligodendroglia. *Glia* 55: 57–64.
42. Garcia, M. C., C. Garcia, M. A. Gijon, S. Fernandez-Gallardo, F. Mollinedo, and M. Sanchez Crespo. 1991. Metabolism of platelet-activating factor in human haematopoietic cell lines: differences between myeloid and lymphoid cells. *Biochem. J.* 273: 573–578.

The FASEB Journal article fj.08-113274. Published online September 8, 2008.
The FASEB Journal • Research Communication

Cysteinyl leukotriene 2 receptor-mediated vascular permeability *via* transendothelial vesicle transport

Michael P. W. Moos,* Jeffrey D. Mewburn,† Frederick W. K. Kan,§ Satoshi Ishii,‖,¶ Manabu Abe,# Kenji Sakimura,# Kyoko Noguchi,‖ Takao Shimizu,‖ and Colin D. Funk*,†,1

*Department of Physiology, †Department of Biochemistry, ‡Division of Cancer Biology and Genetics, Cancer Research Institute, and §Department of Anatomy and Cell Biology, Queen's University, Kingston, Ontario, Canada; ‖Department of Biochemistry and Molecular Biology, Faculty of Medicine, University of Tokyo, Tokyo, Japan; ¶Precursory Research for Embryonic Science and Technology (PRESTO), Japan Science and Technology Agency, Tokyo, Japan; and #Department of Cellular Neurobiology, Brain Research Institute, Niigata University, Niigata City, Japan

ABSTRACT **Cysteinyl leukotrienes (CysLTs) are potent mediators of inflammation synthesized by the concerted actions of 5-lipoxygenase (5-LO), 5-LO-activating protein (FLAP), leukotriene C_4 synthase, and additional downstream enzymes, starting with arachidonic acid substrate. CysLTs produced by macrophages, eosinophils, mast cells, and other inflammatory cells activate 3 different high-affinity CysLT receptors: $CysLT_1R$, $CysLT_2R$, and GPR 17. We sought to investigate vascular sites of $CysLT_2R$ expression and the role and mechanism of this receptor in mediating vascular permeability events. Vascular expression of $CysLT_2R$ was investigated by reporter gene expression in a novel $CysLT_2R$ deficient-LacZ mouse model. $CysLT_2R$ was expressed in small, but not large, vessels in mouse brain, bladder, skin, and cremaster muscle. Intravital, in addition to confocal and electron, microscopy investigations using FITC-labeled albumin in cremaster postcapillary venule preparations indicated rapid CysLT-mediated permeability, which was blocked by application of BAY-u9773, a dual $CysLT_1R/CysLT_2R$ antagonist or by $CysLT_2R$ deficiency. Endothelial human $CysLT_2R$ overexpression in mice exacerbated vascular leakage even in the absence of exogenous ligand. The enhanced vascular permeability mediated by $CysLT_2R$ takes place *via* a transendothelial vesicle transport mechanism as opposed to a paracellular route and is controlled *via* Ca^{2+} signaling. Our results reveal that $CysLT_2R$ can mediate inflammatory reactions in a vascular bed-specific manner by altering transendothelial vesicle transport-based vascular permeability.—Moos, M. P. W., Mewburn, J. D., Kan, F. W. K., Ishii, S., Abe, M., Sakimura, K., Noguchi, K., Shimizu, T., Funk, C. D. Cysteinyl leukotriene 2 receptor-mediated vascular permeability *via* transendothelial vesicle transport. *FASEB J.* 23, 000–000 (2009)**

Key Words: inflammation · intravital microscopy · transgenic mice · caveolae

INFLAMMATION, THE FUNDAMENTAL response of blood vessels and adjacent tissues to injury or abnormal stimulation caused by physical, chemical, or biological agents, is a dynamic complex of cytological and molecular events. The cardinal signs of inflammation—redness, warmth, swelling, and pain—are sometimes accompanied by inhibition or loss of function. Whereas warmth and redness are mainly due to increased blood flow in the affected tissue as a result of vasodilation, swelling is based on enhanced vascular permeability that leads to plasma extravasation and results in edema. This enhanced vascular permeability allows emigration of leukocytes and inflammatory mediators to sites of tissue injury as part of the acute response in tissue healing (1). The local increase in microvascular permeability due to disruption of endothelial integrity after surgery can contribute to death by multiple organ dysfunction syndrome (2). Chronic inflammation that causes protracted vascular hyperpermeability and consequent plasma leakage may be responsible for some of the pathophysiological sequelae in atherosclerosis, arthritis, asthma, and proliferative vitreoretinopathy (3).

Cysteinyl leukotrienes (CysLTs) are among the most active known inflammatory mediators (4). The key enzyme for the synthesis of leukotrienes is 5-lipoxygenase (5-LO), which in combination with the 5-LO-activating protein (FLAP) transforms arachidonic acid into leukotriene A_4, which is further modified by leukotriene C_4 synthase (LTC_4S) to leukotriene (LT) C_4. LTC_4 can be further metabolized to LTD_4 and LTE_4. CysLTs bind to 3 different receptors of the G protein-coupled receptor superfamily: cysteinyl leukotriene receptor subtype 1 ($CysLT_1R$), cysteinyl leukotriene receptor subtype 2 ($CysLT_2R$), and the recently characterized GPR17 (4, 5). The distinct expression patterns of the receptors reveal that they are likely to play separate functions and perhaps be implicated in different aspects of the inflammatory response and cardiovascular

[1] Correspondence: Department of Physiology, 433 Botterell Hall, Stuart St., Queen's University, Kingston, ON K7L 3N6, Canada. E-mail: funkc@queensu.ca

doi: 10.1096/fj.08-113274

disease. There has been recent widespread, heightened interest in the 5-LO/leukotriene pathway with respect to cardiovascular inflammation in atherosclerosis, myocardial infarction, and stroke (6–9). Whereas $CysLT_1R$ has been studied in great detail in relation to asthma and other inflammatory disorders (6), our knowledge of $CysLT_2R$ functions is still rather limited, which is in part due to the lack of a specific receptor antagonist.

Recent data from our laboratory and others have implicated $CysLT_2R$ in vascular inflammatory and permeability events in response to leukotriene administration in acute inflammation and in myocardial ischemia/reperfusion injury (10–12). These studies were carried out with $CysLT_2R$ deficient mice (12), as well as with mice overexpressing human $CysLT_2R$ in vascular endothelium (10), a site where $CysLT_2R$ expression has been observed (11, 13). However, much remains to be learned about the mechanism of these events.

The semipermeable characteristic of the endothelium is crucial for establishing the transendothelial protein gradient (the colloid osmotic gradient) that is required for tissue fluid homeostasis (14). Disruption of the endothelial cell barrier results in increased permeability and vascular leak, and endothelial cells are able to dynamically regulate so-called paracellular and transcellular pathways for transport of plasma proteins, solutes, and liquid (14). Interendothelial junctions consist of a complex array of proteins in series with extracellular matrix constituents that serve to limit the transport of albumin and other plasma proteins by paracellular mechanisms. Transcellular regulation can take place at the level of caveolae, the vesicular carriers filled with receptor-bound and unbound free solutes, or *via* transendothelial channels, fluid phase vesicle, and receptor-mediated transport. Here, we have studied the vascular bed-specific expression pattern of $CysLT_2R$ using a novel $CysLT_2R$ knockout mouse strain in which the reporter LacZ gene has been integrated, as well as the impact of $CysLT_2R$ stimulation on the mechanism of vascular permeability using intravital microscopy.

MATERIALS AND METHODS

Animals

The generation of EC-$CysLT_2R$ transgenic mice has been described previously (10). These mice express 7 copies of the human $CysLT_2R$ coding region under control of the Tie2 promoter/enhancer, integrated in a gene-sparse region of chromosome 6. Hemizygous mice were continuously backcrossed with C57BL/6 mice to obtain equal numbers of transgenic (TG) and wild-type (WT) littermates. $CysLT_2R$ deficient-LacZ mice (KO) were generated by standard gene targeting procedures using C57BL/6 embryonic stem cells (unpublished results) Embryos heterozygous for the genetic modification were transferred from Japan and revived at Queen's University. Littermates of heterozygous offspring (all on a C57BL/6 genetic background) were used in these studies. Sequencing of the *Cysltr2* gene verified that the LacZ coding region was in frame with the start codon of a truncated $CysLT_2R$ open-reading frame that yields a genetic *Cysltr2* disruption and allows use of X-Gal staining as a reporter for native sites of $CysLT_2R$ expression.

Investigation of $CysLT_2R$ expression using the reporter LacZ

Tissues were dissected and fixed in 2% paraformaldehyde/0.2% glutaraldehyde on ice for 30 min. LacZ staining was carried out overnight at 37°C in phosphate-buffered saline (PBS) containing 2 mM $MgCl_2$, 5 mM potassium ferrocyanide trihydrate, 5 mM potassium ferricyanide crystalline, 1 mg/ml X-Gal, and 2.5% dimethyl sulfoxide (DMSO).

Experimental intravital microscopy procedures

Mice were anesthetized with ketamine (150 mg/kg) and xylazine (10 mg/kg), and a catheter was placed in the right jugular vein. The cremaster muscle covering the right testicle was prepared as described in detail elsewhere (15). For Ca^{2+} signaling-related experiments, the cremaster muscle was superfused with Ca^{2+}-free PBS. Microscopic evaluation of postcapillary venules (~17 μm diameter) was recorded throughout the experiment on S-VHS video tape for subsequent data analysis. Initially, bright field images were recorded for 5 min, and blood velocity in the vessel was measured. Fluorescein isothiocyanate (FITC) -labeled albumin (25 mg/kg body weight) was injected *via* the catheter, and fluorescence in the preparation was recorded for at least 5 min. CysLTs (LTC_4 and LTD_4, both at 5 μM) or BAY-u9773 (1 μM) were administered to the superfused vessel. After 5 min, a second treatment with CysLTs or BAY-u9773 was carried out, followed by recording for at least 5 min.

The vessel diameter and blood velocity were measured for each experiment prior to and after treatments but were not modified by any of the different experimental parameters.

To block Ca^{2+} signaling, we added the acetoxymethyl form of the Ca^{2+}-chelator BAPTA (BAPTA-AM; 10 μM) (16) to the suffusion medium and preincubated the cremaster muscle for 15 min before injecting FITC-labeled albumin and prior to CysLT stimulation. In separate experiments, thapsigargin (30 μM final concentration), an inhibitor of the sarco/endoplasmic reticulum Ca^{2+}-ATPase (SERCA), was applied to discharge intracellular Ca^{2+} stores to generate a steady Ca^{2+} signal (17, 18).

To block caveolae/lipid rafts and thereby transcellular vesicle transport, 20 mM methyl-beta-cyclodextrin (MBCD) was added to the suffusate. The cremaster muscle was preincubated for 15 min, followed by CysLT and BAY-u9773 treatment, as described above.

Quantification of vascular permeability

To quantify vascular permeability of postcapillary venules in the cremaster muscle, digital images were stored every 20 s throughout fluorescence recording. The mean fluorescence intensity for each image was measured (gray level range from 0 (black) to 255 (white)).

We calculated a linear function $f(x) = mx + n$ describing the change in fluorescence intensity m over time x for every stage of the experiment (pretreatment and posttreatment). The parameter LIFT (leakage intensity factor for tissues) was calculated as the first equation of this linear function. This LIFT parameter describes the slope of a linear function representing the changes in fluorescence intensity in the tissue over time and is therefore a measure for vascular permeability.

Quantification of FITC-albumin accumulation sites

Sites of FITC-labeled albumin accumulation were initially recorded with a SonyDXC-390m3 CCD color video camera (Sony, Tokyo, Japan). Subsequently, we used a digital camera (ORCA-ER C4742-80-12AG, Hamamatsu Photonics K.K., Hamamatsu City, Japan) to determine the number of accumulating sites at greater resolution and sensitivity. Sites of accumulation of FITC-labeled albumin were determined based on the histogram of the entire image and were counted with Image Pro software (Media Cybernetics, Bethesda, MD, USA).

To allay concern that FITC-labeled albumin accumulation within cells (see Results) does not influence vascular permeability measurements that are based on total brightness of the recorded images, we modeled the effect by using a total black picture (gray level 0) on which 15 white spots (gray level 255 U) sized at 100 pixels were added to represent FITC-albumin accumulation. The change in total brightness (0.28 U) represented by this procedure is comparable to a 12 s measurement from unstimulated WT cremaster muscle preparations. To exaggerate this process we marked the periphery of a typical venule outline white, which caused a brightness change (1.36 U) that resembles only 11 s of recorded leakage from CysLT-stimulated WT preparations. Since the permeability measurements and LIFT parameter were calculated based on a 5 min observation, the contribution of FITC-albumin accumulation sites to LIFT represents less than 3.6% and was therefore regarded as negligible.

Confocal microscopy

Cremaster muscles were collected after intravital microscopy experiments and immediately fixed in 2% paraformaldehyde/0.2% glutaraldehyde on ice for 30 min. The tissue was embedded in Tissue-Tek (Sakura Finetek, Torrance, CA, USA). Cryosections (10 μm) were cut and labeled with pan-endothelial cell antigen antibody MECA-32 (BD Pharmingen, San Diego, CA) and Texas Red conjugated goat anti-rat immunoglobulin G (IgG). Sections were examined using a Leica TCS SP2 multi photon confocal laser scanning microscope (Leica Microsystems, Wetzlar, Germany).

Electron microscopy

For electron microscopic examination of transcytotic vesicles in blood vessels of the cremaster muscle, we followed intravital microscopy procedures as described above. The cremaster muscle was excised and fixed immediately by immersion in 2.5% glutaraldehyde in 0.1 M cacodylate buffer, pH 7.4. After 2 h at 4°C, the tissue samples were washed 3 times with PBS and then trimmed into small pieces for Epon embedding (Epon 812), as described previously (19). One-micrometer-thick sections were first examined by light microscopy in order to locate the area of interest, after which Epon thin sections were cut with a diamond knife on a LKB ultramicrotome and mounted on copper grids. After counterstaining with uranyl acetate and lead citrate solutions, the sections were examined on a Hitachi 7000 electron microscope operated at 75 kV. In randomly taken pictures of postcapillary venules, the area of endothelial cells was measured and the vesicles inside were counted.

Cell culture

Murine b-end.3 endothelial cells were kindly provided by Dr. Yves St. Pierre (University of Quebec, Quebec, QC, Canada). Cells were tested for $CysLT_1R$ (CAGGAGCCCTGTGAATGGAG, GTGGCCACTGTTCTTATGTTG) and $CysLT_2R$ (CGTTCACCAGAAGCAGGGC, CTGAGTGTGGTGCGTTTCCTG) expression by polymerase chain reaction. Cells were subsequently transfected with pcDNA3-huCysLT2R vector (13) and selected with Geneticin (Invitrogen, Carlsbad, CA, USA) to generate stable $huCysLT_2R$ overexpressing cells. Prior to experiments, cells were incubated for 5 min in PBS, followed by addition of FITC-albumin (1.33 μg/ml in PBS), LTC_4/LTD_4 (5 μM in FITC-albumin/PBS), or BAY-u9773 (1 μM in FITC-albumin/PBS). Cells were washed with PBS and fixed in 2% paraformaldehyde/0.2% glutaraldehyde and examined by fluorescence microscopy.

Statistical analysis

For each experimental group, the mean and SE were calculated. To compare groups, we performed 2-sided t tests for independent samples. $P < 0.05$ was considered a statistically significant difference.

RESULTS

$CysLT_2R$ expression in vasculature

Using a novel $CysLT_2R$ deficient-LacZ mouse strain in which the LacZ reporter gene is driven by the *Cysltr2* gene promoter (unpublished results), we assessed vascular $CysLT_2R$ expression with X-Gal blue staining in a variety of organs. No $CysLT_2R$ expression could be detected in the vasculature of lung, intestines, and liver. On the other hand, a few discrete areas of positive staining were detected in blood vessels of the heart and in cardiac tissue after myocardial ischemia/reperfusion injury, and also in vessels of the muscular body wall and diaphragm (11 and data not shown). However, in organs including the bladder, brain/spinal cord, skin, ear, and the cremaster muscle surrounding the testis, strong staining in small vessels was evident, whereas the larger blood vessels were negative (**Fig. 1**). Section analysis revealed staining in the microvasculature within endothelial cells. These results indicate that $CysLT_2R$ expression in the vasculature occurs within the endothelium and is dependent on the organ and vessel size.

Intravital microscopy to assess role of $CysLT_2R$ in vascular permeability

We have recently shown that CysLTs evoke $CysLT_2R$-mediated vascular permeability responses in the ear and in the heart after ischemia/reperfusion injury of TG mice that overexpress human $CysLT_2R$ in vascular endothelium (10, 11). To visualize this process and to assess the importance of endogenous $CysLT_2R$ and CysLTs, we undertook an intravital microscopy study with KO mice as well as with TG and WT C57BL/6 mice using the well-established cremaster muscle preparation. We observed strong endogenous small-vessel $CysLT_2R$ expression (Fig. 1). Fluorescence intensity measurements in vascular preparations from WT and KO mice after administration of FITC-labeled albumin

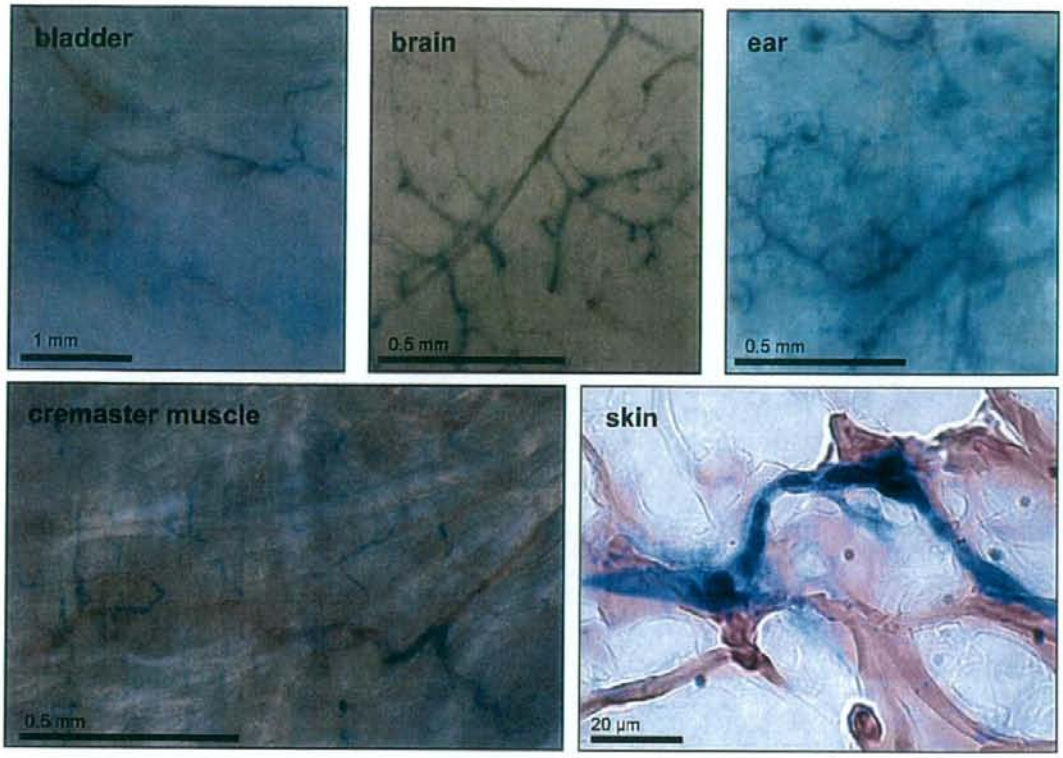

Figure 1. Sites of vascular $CysLT_2R$ expression in various organs using surrogate LacZ reporter gene expression driven by the *Cysltr2* gene promoter. Small vessels within the bladder (top left panel), brain (top middle panel), ear (top right panel), and cremaster muscle (bottom left panel) demonstrate strong X-gal blue positivity indicating $CysLT_2R$ expression, whereas larger blood vessels in these organs show little or no staining. Sectioning of dorsal skin (bottom right panel) reveals strong expression of $CysLT_2R$ in the microvascular endothelium.

revealed a stable pattern, indicating minimal vascular permeability (**Figs. 2** and **3**) that did not change within 20 min in control experiments. Superfusion of the tissue with CysLTs (5 µM each LTC_4/LTD_4) evoked a strong and rapid increase in vascular permeability over 5–15 min, as measured by increasing extravascular fluorescence intensity in WT mice. However, no effect was observed in KO mouse preparations (Figs. 2 and 3). In contrast, TG mice showed evidence, even without exogenous CysLT administration, of increased vascular permeability shortly after FITC-albumin injection, attaining greater than 50% the level observed in CysLT-stimulated WT mice (Figs. 2 and 3). The vessels visualized in these experiments had the same diameter range (WT, 16.9±4.4 µm, n=21; TG, 17.2±2.3 µm, n=22).

Vascular leakage of FITC-albumin by CysLTs could be quenched rapidly to a level where changes in fluorescence intensity are no longer detectable by application of the dual $CysLT_1R/CysLT_2R$ antagonist BAY-u9773 (1 µM; Fig. 3). This effect was observed in vascular preparations from TG and WT mice with and without preceding CysLT stimulation (Fig. 3). BAY-u9773 treatment, on the other hand, had no visible effect on vascular permeability as measured by fluorescence intensity in the vasculature of KO mice (Fig. 3).

In contrast to the high permeability observed in the right cremaster muscle vascular preparation of live TG mice, no signs of immediate vascular permeability (FITC-albumin leakage or FITC-albumin accumulating sites; see below) could be seen in the left cremaster muscle, which was prepared after euthanization to eliminate blood flow- or blood pressure-related effects. This suggests that one possibility for the observed strong vascular permeability response in TG mice in the absence of exogenous ligands was caused by endogenous CysLTs released during the initial surgical intervention interacting with enhanced numbers of $CysLT_2R$ in the endothelium.

$CysLT_2R$ challenge with BAY-u9773 subsequent to vascular permeability elevation leads to endothelial cell accumulation of FITC-albumin

Besides the obvious vascular leakage of FITC-albumin into the extravascular tissue of TG and WT mice, there was evidence for distinct FITC-albumin accumulating

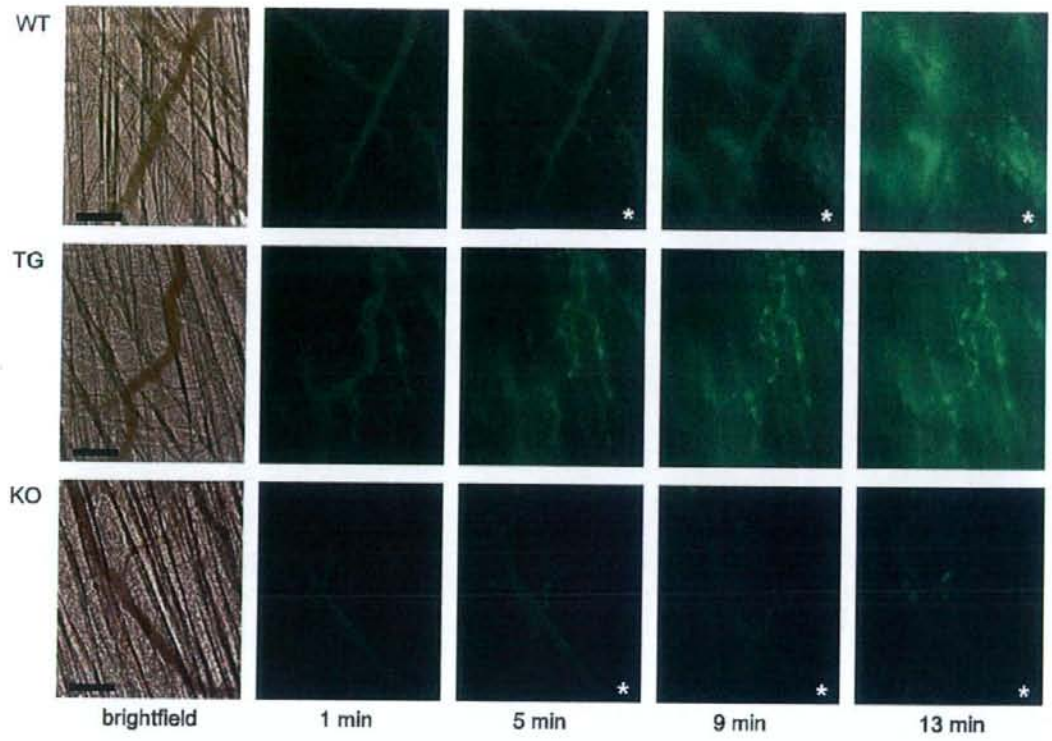

Figure 2. Intravital microscopy recordings of vascular leakage in cremaster muscle postcapillary venules using FITC-labeled albumin. One representative mouse cremaster muscle preparation from each of 3 groups expressing normal (WT, top panels), elevated (TG, middle panels), and no (KO, bottom panels) $CysLT_2R$ are depicted ($n \geq 8$). Leftmost panels show brightfield images; other panels in each row show fluorescence recordings at indicated time points after administration of FITC-labeled albumin *via* a jugular vein catheter. Asterisks indicate period of CysLT superfusion of WT and KO preparations. Scale bars = 50 μm.

bright fluorescent sites (Figs. 2 and **4*A***). These sites are most evident where the leakage of FITC-albumin into the surrounding tissue was initiated and can be used as a marker for number of leakage sites (20). The number of these bright fluorescent sites per unit area was significantly higher in vascular preparations from TG mice compared to WT mice in the absence of exogenous CysLT administration (Fig. 2 and data not shown). CysLT stimulation evoked not only an increase in vascular leakage in WT mice (Figs. 3 and **5**), but also caused a significant increase in the number of these bright accumulation sites. Challenge with BAY-u9773 led to a further significantly increased number of FITC-albumin accumulation sites in both WT and TG mice. These sites are localized in distinct regions on the inner vessel wall, where they can cover almost the whole vessel after BAY-u9773 treatment, as shown in Fig. 4*A*. The location and pattern of the FITC-albumin bright sites implies that endothelial cells after $CysLT_2R$ stimulation initiate vascular permeability by a transcellular pathway rather than at interendothelial gap junctions. These results also indicate that $CysLT_2R$ challenge with BAY-u9773 restores the barrier function of the endothelium by blocking exocytosis at the abluminal site of the endothelium which is shown by an increase in accumulation of albumin at sites of prior high vascular permeability (Fig. 5). This hypothesis is supported by the fact that when vascular preparations from WT and TG mice were first pretreated with BAY-u9773, followed by subsequent stimulation with CysLTs, there was a sudden increase in fluorescence intensity. Therefore, after CysLT treatment, stored fluorescent albumin within endothelial cells was suddenly released. This reaction was quite unique and could not be reproduced by CysLT treatment alone or by a second BAY-u9773 addition (data not shown).

Examining this in further detail, confocal laser scanning images revealed accumulation of FITC-albumin within endothelial cells (positive for the pan-endothelial cell marker Meca-32) of blood vessels after CysLT stimulation (Fig. 4*B*), indicating transcellular transport. Moreover, electron microscopy analysis of CysLT- and BAY-u9773-treated postcapillary venules revealed a significantly increased number of vesicles inside the endothelium compared to unstimulated venules (**Fig. 6**), suggesting an increase in vesicle formation and/or transport in response to CysLT stimulation.

To mimic the *in vivo* setting within endothelial cells

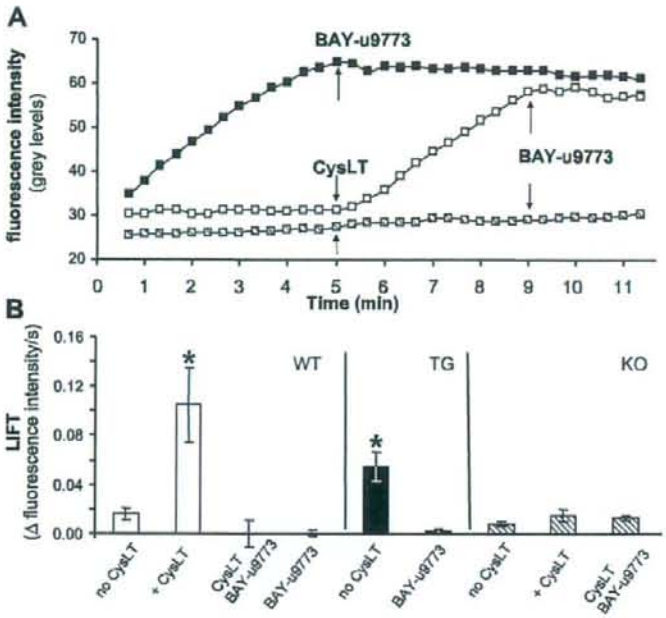

Figure 3. $CysLT_2R$ mediates vascular permeability in cremaster muscle postcapillary venules. *A*) Representative measurements of fluorescence intensity in cremaster muscle preparations from WT (open boxes), TG (filled boxes), and KO (striped boxes) mice used to calculate FITC-albumin leakage. After i.v. FITC-albumin administration, WT and KO mouse preparations were treated after 5 min with LTC_4/LTD_4 (CysLT) superfusion and 4 min later with the dual $CysLT_1R/CysLT_2R$ antagonist BAY-u9773. Autogenous leakage in TG preparations was blocked by treatment with BAY-u9773 after 5 min. Neither CysLTs nor BAY-u9773 treatment of KO mouse preparations caused changes in vascular leakage. *B*) LIFT parameter (mean+SE; see Materials and Methods) was calculated for several experimental conditions: no CysLT treatment (n=17, WT; n=14, TG; n=8, KO); with CysLT (5 μM) stimulation (n=10, WT; n=8, KO); after BAY-u9773 (1 μM) with preceding CysLT stimulation (n=6, WT; n=8, KO); or only with BAY-u9773 treatment (n=6, WT and TG). LIFT is significantly higher (P<0.01) in CysLT-stimulated WT and unstimulated TG vascular preparations compared to the other groups. BAY-u9773 treatment reduced LIFT to almost 0 in WT and TG mice, whereas neither CysLT nor BAY-u9773 treatment of KO mouse vascular preparations showed any change in leakage compared to untreated conditions.

of TG mice in a tissue culture model, b-end.3 mouse endothelial cells were permanently transfected with human $CysLT_2R$ ($CysLT_2R$ b-end.3) and tested for fluorescent albumin accumulation (Fig. 4*C*). We determined that native endothelial cell line b-end.3 expresses neither $CysLT_1R$ nor $CysLT_2R$, and these cells do not accumulate FITC-albumin even after stimulation with CysLTs or BAY-u9773. $CysLT_2R$ b-end.3 cells, on the other hand, showed a significant number of labeled-albumin accumulating cells after treatment with CysLTs or BAY-u9773. Together, these data indicate that $CysLT_2R$ modulation leads to endothelial cell albumin uptake.

$CysLT_2R$-induced vascular permeability is mediated by Ca^{2+} signaling

$CysLT_2R$ stimulation in endothelial cells has been linked to oscillating calcium signals of unknown functional significance (21). The inhibition of intracellular Ca^{2+} signals by BAPTA prevented enhanced vascular permeability elicited by CysLT stimulation in WT cremaster muscle preparations (Fig. 5). This indicates that intracellular Ca^{2+} signals are essential for $CysLT_2R$-regulated vascular permeability.

Thapsigargin causes the release of Ca^{2+} from intracellular stores by blocking SERCA, thereby creating a

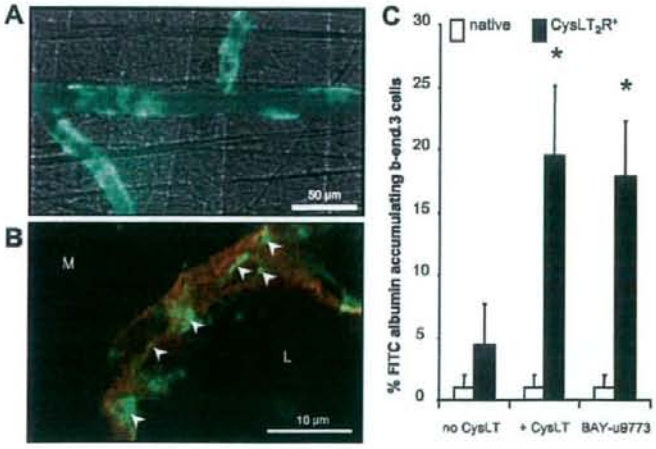

Figure 4. FITC-labeled albumin accumulation *in vivo* and *in vitro* affected by $CysLT_2R$ activation and BAY-u9773. *A*) Merge of fluorescence and phase-contrast images of postcapillary venules from a TG mouse revealing FITC-albumin accumulation along the inner vessel wall after BAY-u9773 treatment. *B*) Confocal laser scanning image showing FITC-labeled albumin (green) inside Meca32/Texas Red-labeled endothelium (red), blood vessel lumen (L), and surrounding muscular tissue (M); white arrowheads point to intracellular FITC-albumin accumulation. *C*) FITC-albumin accumulation in native and human $CysLT_2R$ transfected b-end.3 murine endothelial cells was examined after stimulation with CysLTs or BAY-u9773. While native cells, which do not express CysLT receptors, fail to accumulate FITC-albumin, the transfected cells do so after both treatments. *P < 0.05 *vs.* native cells; n = 3.

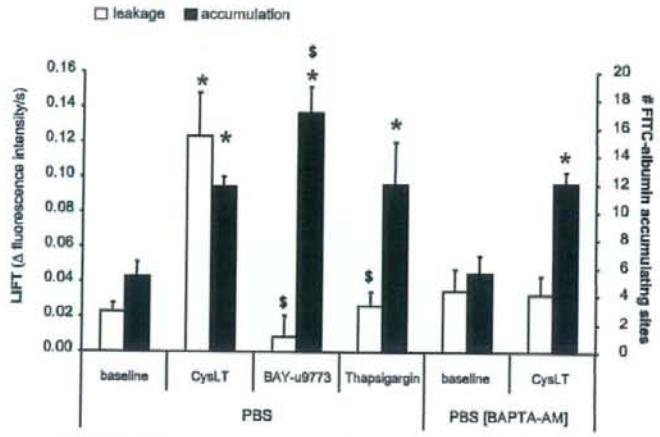

Figure 5. Endothelial vascular leakage sites affected by $CysLT_2R$-activated Ca^{2+} signaling. Vascular permeability (LIFT; white bars) was calculated and FITC-labeled albumin accumulating sites were counted (black bars) in WT cremaster muscle preparations for several experimental conditions: WT mice without treatment (n=17 LIFT/n=7 hot spots); after stimulation with LTC_4/LTD_4 (n=12/n=4); LTC_4/LTD_4-prestimulated preparations followed by BAY-u9773 (n=7/n=3); treatment with thapsigargin (n=5/n=3); and BAPTA preincubation with (n=7/n=3) and without LTC_4/LTD_4 stimulation (n=6/n=3). CysLT-induced heightened vascular permeability is inhibited by BAY-u9773 and the Ca^{2+} chelator BAPTA. The steady Ca^{2+} signal released by thapsigargin does not induce vascular permeability alterations but leads to FITC-albumin accumulation in the endothelium. FITC-labeled albumin accumulation is triggered by CysLT stimulation regardless of BAPTA treatment and can be further increased with the dual $CysLT_1R$/$CysLT_2R$ antagonist BAY-u9773. Data are means ± SE; $^*P < 0.05$ *vs.* baseline; $^\$P < 0.05$ *vs.* CysLT stimulation.

steady Ca^{2+} signal. However, in these experiments (Fig. 5), treatment with thapsigargin did not lead to an increase of vascular permeability, indicating that a steady Ca^{2+} signal is not sufficient to provoke vascular leakage. While thapsigargin did not elevate vascular permeability, its application led to an increased number of FITC-labeled albumin accumulation sites in the absence of CysLT administration. This signifies that thapsigargin may induce endothelial luminal endocytosis, but not abluminal exocytosis. The fact that BAPTA blocked vascular permeability but only marginally influenced the number of CysLT-stimulated FITC-albumin accumulation sites (Fig. 5) reveals that the Ca^{2+}-buffering capacity of BAPTA is important for setting weaker oscillating Ca^{2+} signals, as described previously in *Xenopus* melanotropes (22), which might influence exocytosis of labeled-albumin from the vascular endothelial cells into the extravascular space.

Blockade of caveolae and subsequent vesicle formation with MBCD attenuates transcytosis of albumin in response to CysLT stimulation

Caveolae are known to transport albumin and other plasma proteins across the endothelium, and it is at these sites that vesicles are derived for transcytosis (14). Inhibition of caveolae/lipid rafts by application of MBCD resulted in significantly decreased baseline vascular permeability (LIFT=0.002±0.002; n=8; P<0.01, +MBCD *vs.* −MBCD) and a significantly delayed response to CysLT stimulation (**Fig. 7*B***). The CysLT-induced increase of vascular permeability (LIFT=0.121±0.018; n=8) could not be inhibited by application of BAY-u9773 (LIFT=0.110±0.027; n=4), as observed in cremaster muscle preparations not treated with MBCD (Fig. 7*A*; compare Fig. 3). However, the bright fluorescent accumulation of albumin within endothelial cells was blocked by MBCD (Fig. 7*C*). These results

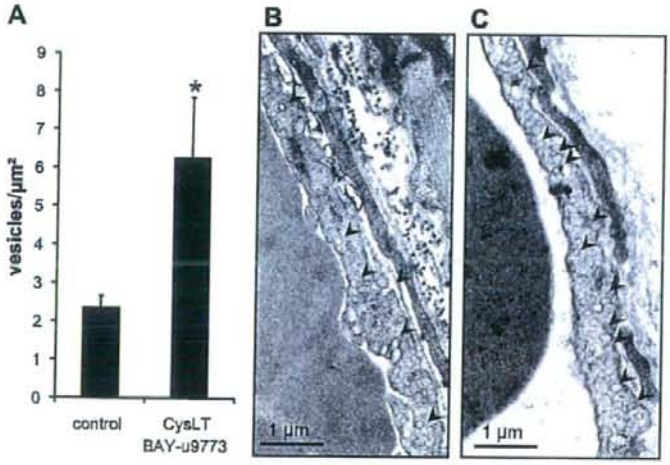

Figure 6. $CysLT_2R$-mediated transendothelial vesicles. *A*) Vesicles per unit area in endothelial cells counted on electron microscopy images of cremaster muscle sections taken after intravital microscopy experiments treated with CysLT and BAY-u9773. Contralateral untreated cremaster muscle was used as a control. CysLT/BAY-u9773-treated cremaster muscle sections show a significantly increased number of vesicles compared to controls. $^*P < 0.05$; n = 8. *B, C*) Representative electron microscopy images of a section from a control (*B*) and a CysLT/BAY-u9773-treated cremaster muscle (*C*) with vessel lumen toward the left. Black arrowheads point to vesicles in the endothelial cell.

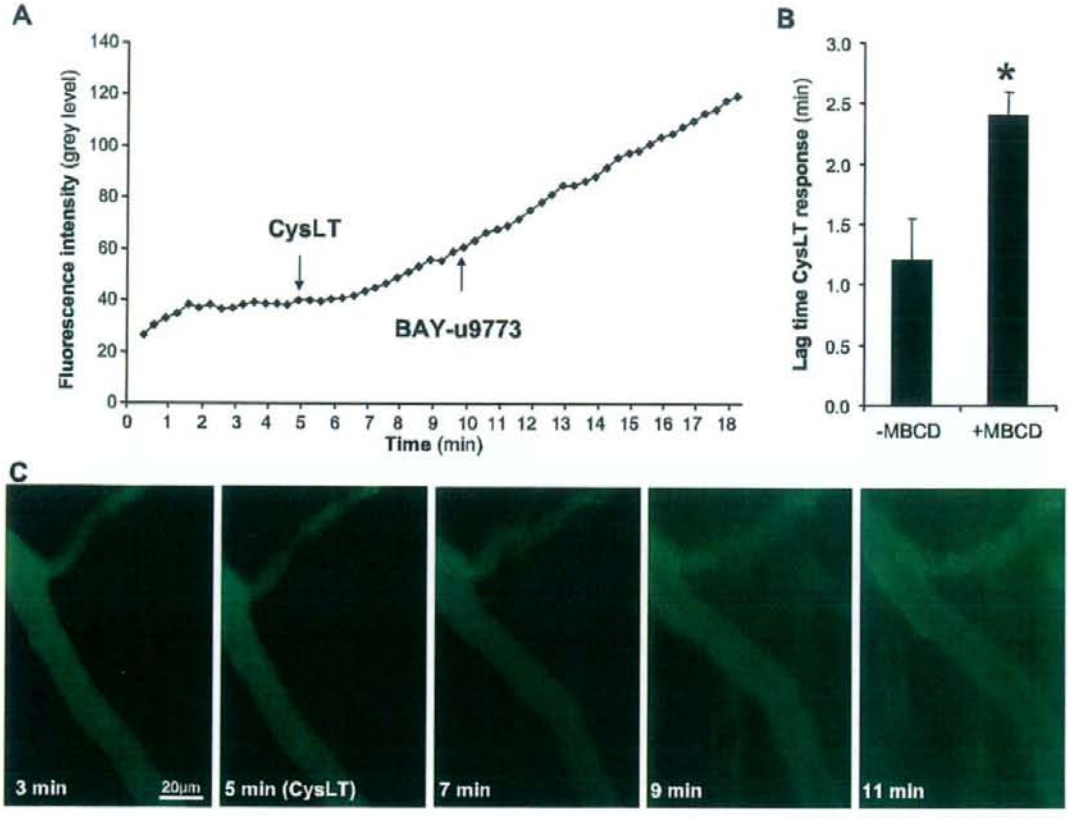

Figure 7. Inhibition of caveolae with MBCD causes a time-delayed vascular permeability response without FITC-albumin accumulation in the vessel wall. *A*) Representative measurements of fluorescence intensity in a cremaster muscle preparation from a WT mouse preincubated for 15 min with MBCD. After i.v. FITC-albumin administration, CysLTs stimulate an increase of fluorescence with a lag time of 2 min that is not influenced by subsequent application of BAY-u9773. *B*) CysLT response lag time for WT mice cremaster muscles with (+) MBCD preincubation is significantly increased compared to non-MBCD treated (−) mice. $n = 6$; $^*P < 0.05$. *C*) Representative series of images from an MBCD-pretreated cremaster muscle. Leakage starts 2 min after application of CysLT without establishing FITC-albumin accumulation sites within the vessel wall.

indicate that blockade of caveolae inhibits transcytosis but may activate a compensatory paracellular transport mechanism, as recognized in caveolin-1 null mice (23).

DISCUSSION

The first analysis of $CysLT_2R$ KO mice (12) and TG mice overexpressing human $CysLT_2R$ in vascular endothelium (10) indicated a potential role for $CysLT_2R$ activation to increase vascular permeability. In the present study, we explored this facet in greater detail by means of intravital/confocal/electron microscopy imaging combined with a determination of vascular sites of $CysLT_2R$ expression. Our findings indicate an organ and blood vessel specificity of $CysLT_2R$ expression and that in cremaster muscle postcapillary venules, $CysLT_2R$ is the major leukotriene receptor subtype involved in the control of vascular permeability through a transcellular transport pathway. The fact that the permeability response in this vascular bed was absent in $CysLT_2R$ KO mice indicates that neither $CysLT_1R$ nor the newly discovered CysLT receptor known as GPR17 (5) participate in this activity. These results reveal a key role for $CysLT_2R$ in vascular responses to injury, such as that observed after myocardial infarction/reperfusion, as we have reported recently (11).

In the cremaster muscle preparation, TG mice displayed enhanced vascular permeability without exogenous ligand administration, whereas in WT mice this could only be observed after stimulation with CysLTs. These observations suggest that TG mice would develop massive edema, which has not been observed previously. In ear inflammation models, either exogenous CysLT administration was required (direct model) or an induction of CysLT synthesis was necessary (passive cutaneous anaphylaxis model) (10). No signs of enhanced vascular permeability/FITC-albumin leakage or FITC-albumin accumulating leakage sites could be observed in the contralateral (left) cremaster muscle of WT or TG mice immediately after euthanization. This

leads us to surmise that in TG mice the observed hyperpermeability vascular response might be due to the surgical intervention; presumably, low levels of CysLT are produced by resident tissue macrophages and/or mast cells during preparation of the cremaster muscle on the microscope stage. Because of the enhanced numbers of $CysLT_2R$ binding sites within the vascular endothelium of TG mice, they are likely more sensitive to CysLTs and therefore respond to endogenous CysLTs to a much greater degree than WT mice. An alternative, albeit less likely, interpretation is that the overexpressed $CysLT_2R$ is constitutively active in some vascular beds, although the ligand-independent activation of GPCRs and constitutive activity *in vivo* have been difficult to verify (24).

FITC-albumin extravasation from the venules is initiated and takes place at certain "hot spots" of fluorescence accumulation called "leaky sites" by Huang *et al.* (20). In our studies, these sites were observed in discrete regions throughout the endothelium. They have been observed by intravital microscopy in response to burns (20), platelet-activating factor/leukotriene B_4 (25), and CysLTs (herein), but not in response to many other stimuli, such as histamine (26), tumor necrosis factor α (27), and homocysteine (28). Electron microscopy observations of albumin extravasation have revealed that it is mediated mainly by transcellular vesicle transport (14, 29 and Fig. 6). Furthermore, pinocytotic vesicular transport appears to be a primary means by which luminal to abluminal transport occurs in response to bradykinin/LTC_4 stimulation to enhance vascular permeability in certain vessels in rat brain (30). BAY-u9773, an antagonist of both $CysLT_1R$ and $CysLT_2R$, functions at lower concentrations as a partial agonist of $CysLT_2R$ (31). In our study, BAY-u9773 superfusion of the tissue may elicit an initial stimulation of $CysLT_2R$ (transcellular vesicle transport mechanism initiation), followed by antagonist activity (FITC-albumin accumulation; **Fig. 8**). In line with this reasoning, after inhibition of $CysLT_2R$ with BAY-u9773 followed by subsequent stimulation with CysLTs, a very strong, immediate abluminal release of FITC-albumin into the extravascular compartment is observed. Interestingly, the absence of FITC-albumin accumulation in the vessel wall of MBCD-pretreated vessels after CysLT stimulation (Fig. 7*C*) further supports that blockade of caveolae, and subsequent vesicle formation attenuates CysLT-induced transcytosis and perhaps initiates a compensatory switch to paracellular transport, as has been described previously for caveolin-1 null mice (23). This point will have to be verified in future experiments.

Calcium signaling in acute vascular hyperpermeability responses (*e.g.*, histamine) is well-recognized *via* Ca^{2+}-calmodulin initiation of a cascade leading to contraction of endothelial cells and opening of intercellular junctions (14). Prolonged signaling (*e.g.*, thrombin) generates similar cellular events, as well as protein tyrosine phosphorylation and RhoA activation (32). Ca^{2+} signaling in transcellular vesicle transport-mediated vascular hyperpermeability has been postulated but never rigorously proven (14). Nevertheless, some clues have been collected. For example, vascular endothelial growth factor (VEGF) has been shown to stimulate enhanced vascular permeability *via* transcellular vesicles, and Ca^{2+} signals seem to be involved in forming, joining, and releasing the vesicles (33). Recent studies have demonstrated that CysLT stimulation of human umbilical vein endothelial cells predominantly expressing the $CysLT_2R$, as opposed to $CysLT_1R$, causes a potent Ca^{2+} spike followed by an oscillating Ca^{2+} signal (21). Taking into account the increased number of FITC-albumin accumulating sites after CysLT + BAY-u9773 treatment, thapsigargin addition, or CysLT stimulation in BAPTA-pretreated vessels, we speculate that an initial Ca^{2+} signal evoked by CysLT stimulation of $CysLT_2R$ leads to vesicle formation and endocytosis at luminal sites of endothelial cells (Fig. 8) similar to the VEGF model described by Bates (33). The $CysLT_2R$-triggered oscillating Ca^{2+} signal described

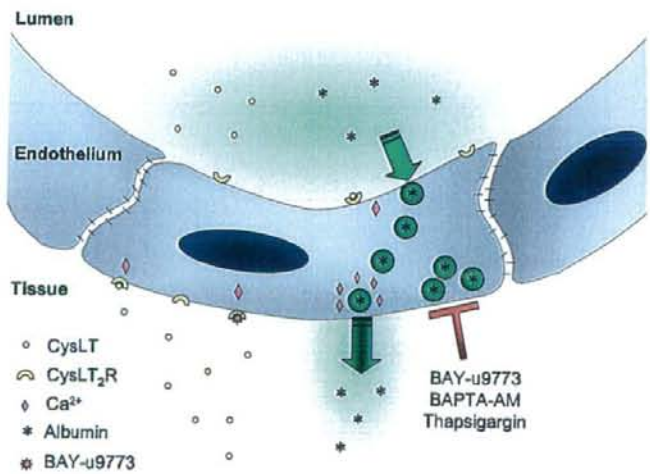

Figure 8. Model of $CysLT_2R$-regulated vascular leakage. Activation of $CysLT_2R$ by CysLTs or by the partial agonist activity of BAY-u9773 (31) results in a Ca^{2+} signal in the endothelial cell, which can also be mimicked by thapsigargin treatment. This Ca^{2+} signal stimulates vesicle formation and endocytosis at the luminal side, allowing the cell to accumulate albumin. The albumin-filled vesicles are transported to the abluminal side. Exocytosis of the albumin-filled vesicles and resultant vascular hyperpermeability is likely triggered by an oscillating Ca^{2+} signal (21) that is induced by CysLT-stimulation of the $CysLT_2R$. This oscillating Ca^{2+} signal can be blocked by the $CysLT_2R$ antagonist activity of BAY-u9773, by intracellular chelation with BAPTA, or by emptying intracellular stores with thapsigargin. This prevents exocytosis and causes an accumulation of albumin-filled vesicles inside the endothelial cell.